Molecular Cell

Article

G3BP1 promotes intermolecular RNA-RNA interactions during RNA condensation

Graphical abstract

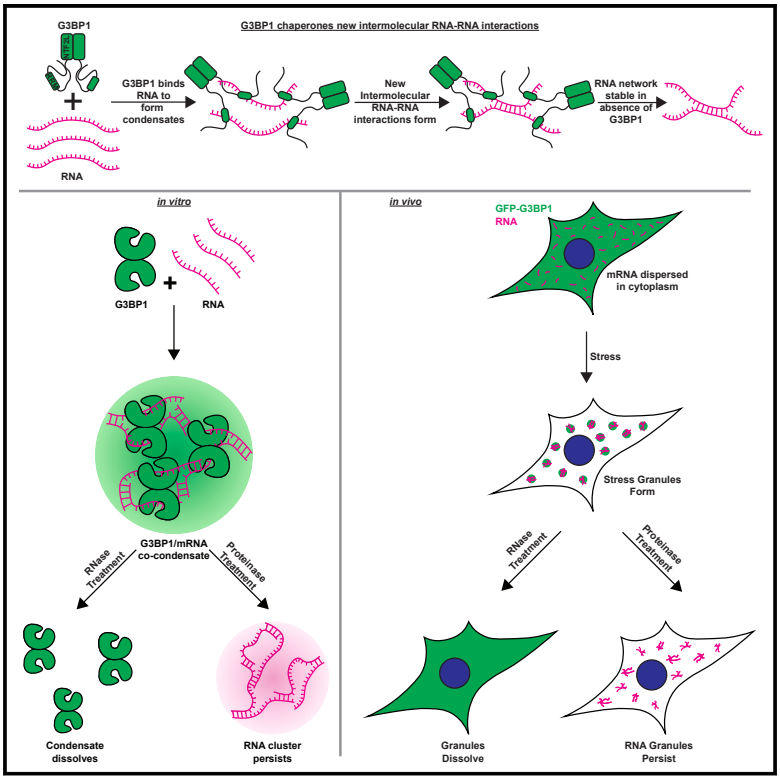

Highlights

- G3BP1 promotes the formation of intermolecular RNA-RNA interactions *in vitro*
- Base-pairing interactions contribute to RNA-RNA interaction stability
- Stress granules and nucleolar RNAs persist in assemblies without protein scaffolds
- G3BP1 can act as a condensate chaperone

Authors

Dylan M. Parker, Devin Tauber, Roy Parker

Correspondence

roy.parker@colorado.edu

In brief

Parker et al. demonstrate that some proteins responsible for organizing ribonucleoprotein granules can chaperone intermolecular RNA-RNA interactions in addition to their role in scaffolding. These findings cement RNA-RNA interaction networks as a key component of granules, highlighting the need to further explore the regulation of RNA dynamics within granules.

Parker et al., 2025, Molecular Cell *85*, 571–584
February 6, 2025 © 2024 The Author(s). Published by Elsevier Inc.
https://doi.org/10.1016/j.molcel.2024.11.012

CellPress

Molecular Cell

CellPress
OPEN ACCESS

Article

G3BP1 promotes intermolecular RNA-RNA interactions during RNA condensation

Dylan M. Parker,[1,2] Devin Tauber,[1] and Roy Parker[1,2,3,*]
[1]Department of Biochemistry, University of Colorado Boulder, Boulder, CO 80309, USA
[2]Howard Hughes Medical Institute, University of Colorado Boulder, Boulder, CO 80309, USA
[3]Lead contact
*Correspondence: roy.parker@colorado.edu
https://doi.org/10.1016/j.molcel.2024.11.012

SUMMARY

Ribonucleoprotein (RNP) granules are biomolecular condensates requiring RNA and proteins to assemble. Stress granules are RNP granules formed upon increases in non-translating messenger ribonucleoprotein particles (mRNPs) during stress. G3BP1 and G3BP2 proteins are proposed to assemble stress granules through multivalent crosslinking of RNPs. We demonstrate that G3BP1 also has "condensate chaperone" functions, which promote the assembly of stress granules but are dispensable following initial condensation. Following granule formation, G3BP1 is dispensable for the RNA component of granules to persist *in vitro* and in cells when RNA decondensers are inactivated. These results demonstrate that G3BP1 functions as an "RNA condenser," a protein that promotes intermolecular RNA-RNA interactions stabilizing RNA condensates, leading to RNP granule persistence. Moreover, the stability of RNA-only granules highlights the need for active mechanisms limiting RNP condensate stability and lifetime.

INTRODUCTION

Biomolecular condensates, often composed of RNA and protein components, are a fundamental mode of cellular organization.[1–3] Biomolecular condensates are associated with diverse cellular functions including RNA metabolism, protein complex assembly, and cell-fate specification.[4–7] The dysregulation of condensates impacts infectious disease, neurodegeneration, and cancer.[8–16] Though their composition is condensate-specific, reoccurring physical principles underlie condensate formation, including dependence on multivalent interactions, long-disordered biopolymers, and dynamic exchange with the condensate surroundings.[1–3] However, how condensates are assembled and regulated remains to be fully determined.

Stress granules (SGs) are biomolecular condensates that form from non-translating messenger ribonucleoprotein particles (mRNPs) under translation-limiting conditions.[17–19] SG assembly occurs through protein-protein, protein-RNA, and intermolecular RNA-RNA interactions between mRNPs.[17–19] Under most stress conditions, the paralogs G3BP1 and G3BP2 are essential for SG assembly.[20–24] With the increase in non-translating mRNP concentration upon cellular stress, G3BP dimers bind RNA to facilitate the formation of large intermolecular RNP networks, leading to mesoscale condensates, cellular signaling, and cell resilience.[17,19,25]

G3BP1 can act as an RNA-triggered molecular switch to induce SG formation. Untranslated mRNA facilitates the conformational switching of intrinsically disordered regions in G3BP1 from an autoinhibited state to an RNA-bound, phase-separation-competent dimer.[20–22] Due to G3BP1's promiscuous RNA binding, individual mRNAs can then interact with multiple G3BP1 dimers to form a crosslinked network of G3BP1::RNA interactions, ultimately leading to SG formation.

Several observations led us to test a related model wherein G3BP1 proteins promote SG formation by forming a high local RNA concentration, promoting the formation of intermolecular RNA-RNA interactions that contribute to SG persistence. First, RNA alone can form stable granules at approximately physiological salt concentrations, and RNA self-assembly can mirror the composition of the endogenous SG transcriptome.[26,27] These observations suggest that the intrinsic property of mRNAs to form RNA condensates largely determines the RNAs recruited to SGs. Second, while condensate scaffolds are typically nondynamic,[28–30] G3BP1 is highly dynamic in SGs *in vivo*.[20,22,31] This property suggests that G3BP1 is either a dynamic scaffold or may not be the primary scaffold of SGs. Third, observations of RNA self-assembly and theory both suggest that the high concentration of RNA in RNP granules would be poised to form new intermolecular RNA-RNA interactions.[32,33] Indeed, in the absence of active mechanisms to limit interactions, such assemblies appear to form non-uniform, extended networks of interactions, trapping molecules in condensate assemblies.[4,26,34–36] Consistent with this process, individual RNA molecules within SGs maintain a

This is an open access article under the CC BY license (http://creativecommons.org/licenses/by/4.0/).

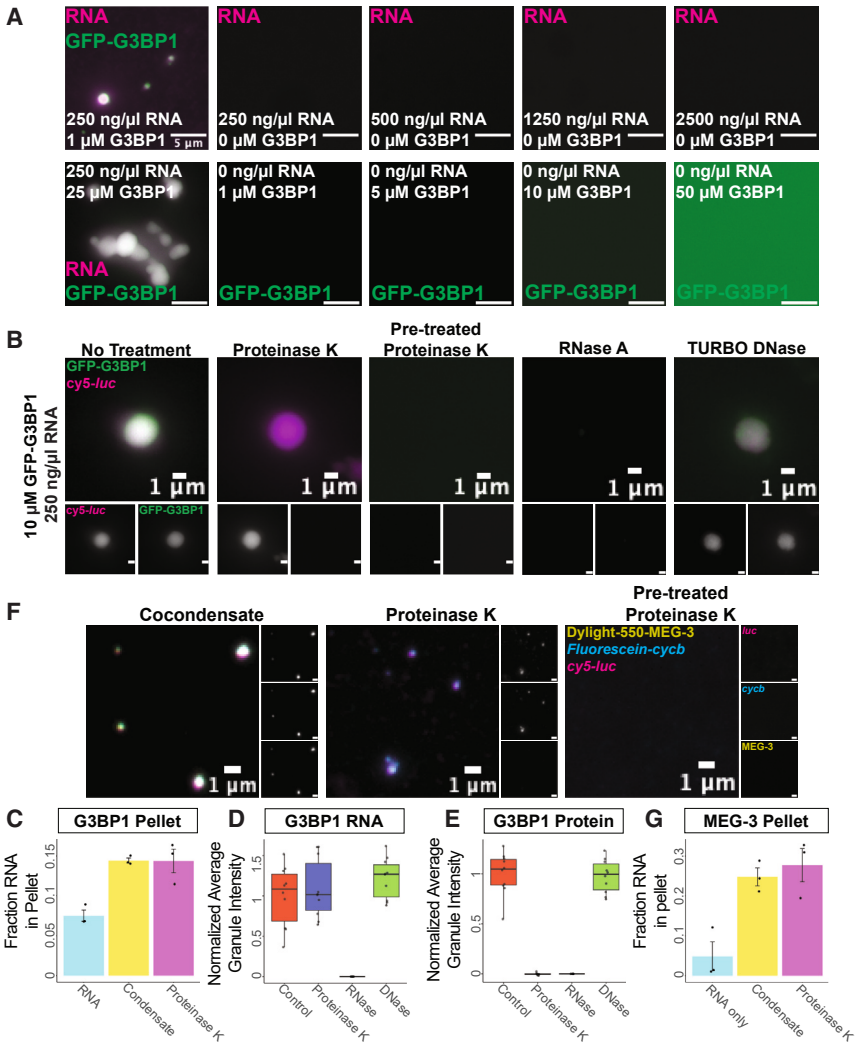

Figure 1. RNA granules persist after degradation of G3BP1

(A) GFP-G3BP1 (green) protein alone, RNA (magenta) alone, or GFP-G3BP1 and RNA were added to condensation buffer (1× PBS with 10 mM $MgCl_2$). RNA samples consist of 50 ng/µL cy5-*luciferase* RNA, with the remaining concentration comprising total U2OS RNA. All scale bars are 5 µm.

(B) G3BP1::RNA co-condensates were formed using 10 µM GFP-G3BP1 (green), 200 ng/µL total hRNA, and 50 ng/µL cy5-labeled *luciferase* RNA (magenta) and hardened for 1 h. Co-condensates were then treated with equal volumes enzyme buffer (STAR Methods), PK (0.1 U/µL), RNase A (1.43 µg/µL), or TURBO DNase (0.28 U/µL) for 15 min before imaging. The pretreated sample (middle) was made by incubating 10 µM GFP-G3BP1 with 0.1 U/µL PK for 15 min before adding to the condensate reaction. All scale bars are 1 µm.

(C) RNA alone, G3BP1::RNA co-condensates, or PK-treated samples were pelleted by spinning for 20 min at 20,000 × *g*, and the fraction of RNA in the pellet was quantified (STAR Methods). Error bars represent the standard deviation.

(D and E) Normalized average RNA (D) and GFP-G3BP1 (E) intensities in condensates from 10 images from 3 experiments performed in (B). All samples were normalized to the average control granule intensity across all images. DNase controls were performed independently and normalized to a separate control set.

(F) MEG-3::RNA co-condensates were formed and treated with PK as with G3BP1::RNA co-condensate in (B), with the exception that 300 nM MEG-3 (yellow) was used, and 50 ng/µL fluorescein-labeled *cycb* RNA (cyan) was added in addition to cy5-*luciferase* (magenta). All scale bars are 1 µm.

(G) RNA alone, MEG-3::RNA co-condensates, or PK-treated samples were pelleted and quantified as in (C). Error bars represent the standard deviation.

See also Figures S1 and S2.

consistent relative position with one another in live-cell imaging experiments.[37]

Herein, we demonstrate that G3BP1 promotes the formation of new intermolecular RNA-RNA interactions, a role defined as an RNA condenser.[32] First, we show that G3BP1 catalyzes the formation of RNA-RNA interactions *in vitro*, leading to RNA granules that can persist following the removal of G3BP1. These G3BP1-depleted RNA granules are sensitive to RNA denaturants and stabilized by crosslinking of RNA duplexes, supporting a role for intermolecular RNA-RNA interactions in granule stability. Strikingly, SGs within human cells disassemble with RNase treatment but persist following degradation or inactivation of G3BP, provided RNA decondensers are also inactivated. These observations argue that balancing the RNA chaperone-mediated formation and decondenser-mediated dissolution of intermolecular RNA-RNA interactions is fundamental to organizing SGs and possibly RNP granules more broadly. This also suggests that proteins required for RNP granule assembly do not necessarily function as scaffolds per se but can instead act as condensate chaperones to promote scaffolding interactions of other molecules, including RNA.

RESULTS

G3BP1 is required for assembly, but not persistence, of RNA granules *in vitro*

To test whether G3BP1 condenses RNA, we assembled co-condensates of G3BP1 and RNA *in vitro*. Similar to earlier work,[20–22] we observed that adding increasing amounts of recombinant GFP-G3BP1 to 200 ng/µL total human RNA (hRNA) caused the formation of G3BP1::RNA co-condensates (Figures 1A and S1A–S1C). The RNA component of G3BP1::RNA assemblies was visualized using 50 ng/µL fluorescently labeled *luciferase* RNA. Under these conditions, GFP-G3BP1::RNA co-condensates appear as micron-scale spherical condensates or reticulated networks of partially fused condensates (Figure 1A, bottom left). Similarly, GFP-G3BP1 forms co-condensates when mixed with oligo(dT)-bead enriched poly(A) RNA[20] or single species of

mRNAs (Figure S1D), but not poly(A)-depleted RNA.[20] In contrast, high concentrations of RNA or GFP-G3BP1 alone do not form granules in these conditions (Figure 1A). These observations are consistent stress-induced polysome release of mRNAs and subsequent condensation by G3BP1 promoting SG formation.

Two overlapping, non-exclusive mechanisms could explain the co-assembly of RNA and G3BP1. First, as supported by previous work, RNA could induce conformational changes in G3BP1, enhancing G3BP1 interactions and thereby triggering protein-driven demixing and liquid-liquid phase separation.[20–22] In a complementary mechanism, the dimerization of two G3BP1 proteins bound to different RNAs could bring those RNA molecules into proximity and promote the formation of new intermolecular RNA-RNA interactions. In this mechanism, G3BP1 functions as an RNA condenser.[32]

To test if G3BP1 could function as an RNA condenser, we examined the stability of GFP-G3BP1::RNA co-condensates following Proteinase K (PK) treatment. If G3BP1 is required to maintain interactions between RNAs as a crosslinking protein, PK treatment should disrupt the RNA assembly. In contrast, if G3BP1 functions as an RNA condenser to promote intermolecular RNA-RNA interactions stabilizing RNP granules, PK digestion should lead to the persistence of RNA assemblies.

A striking result was that RNA assemblies persisted, even after PK treatment of co-condensates degraded the GFP-G3BP1 signal (Figures 1B–1E and S1). In contrast, pre-treatment of the GFP-G3BP1 with PK before mixing with RNA prevented the formation of condensates, indicating that protease treatment is sufficient to degrade the condensation function of G3BP1 (Figure 1B). Pelleting experiments demonstrate that ~15% of RNA is found in the pellet fraction in both intact condensates and protease-treated samples (Figure 1C). Treatment of co-condensates with RNase A completely disperses both RNA and protein signal (Figures 1B–1E). As expected, DNase I treatment did not dissolve GFP-G3BP1::RNA co-condensates (Figures 1B, 1D, and 1E). SDS-PAGE and native agarose gel electrophoresis indicate robust degradation of protein or RNA when treated with proteinase or RNase, respectively (Figure S2). This degradation suggests that GFP-G3BP1-depleted RNA granules observed in microscopy are not due to the degradation of GFP alone, nor does a protease-resistant fragment of G3BP1 scaffold them. Though G3BP1 and RNA are both essential for initial condensate formation, these enzymatic treatments reveal a stable, protein-independent RNA granule forms in G3BP1::RNA co-condensates.

MEG-3 is required for assembly, but not persistence, of RNA condensates *in vitro*

To examine if other RNP granule protein "scaffolds" are only required for initial RNA and protein co-condensation *in vitro*, we examined the assembly of RNA with the MEG-3 protein. In *Caenorhabditis elegans*, germ granules are primarily scaffolded by two protein pairs: MEG-3/4 and PGL-1/3.[38–40] The Seydoux lab recently demonstrated that MEG proteins are essential for recruiting RNA to germ granules, whereas the PGL proteins organize granules throughout development.[29,38,41] Therefore, we purified the MEG-3 protein to test whether another RNP granule scaffolding factor could act as an RNA condenser.

Upon condensation with RNA *in vitro* and subsequent PK treatment, we determined that MEG-3 also promotes the formation of stable RNA assemblies. By mixing MEG-3 with RNA as previously described, we recapitulated the known condensation behaviors of MEG-3, with ~25%–30% of RNAs condensed with MEG-3 based on pelleting (Figures 1F and 1G).[29] Remarkably, when MEG-3::RNA co-condensates were treated with PK, RNA assemblies persisted, and similar amounts of RNA were isolated in particles by pelleting (Figures 1Fand 1G). In contrast, treating MEG-3 with PK before granule assembly prevented the formation of observable granules. The capacity of MEG-3 to form stable RNA assemblies *in vitro* suggests that RNA condenser activity is not unique to G3BP1 and may be a conserved feature of RNP granule nucleating factors, which we further examined in the context of G3BP1.

RNA persistence within PK-treated *in vitro* co-condensates requires aging

The observation that RNA granules remain following the degradation of G3BP1 suggests that the high local concentrations of RNA within the initial protein-RNA co-condensates allow for the formation of new intermolecular RNA-RNA interactions, leading to a stable RNA-RNA interaction network. The rearrangement of RNA from a dynamic state to a stable network within condensates, known as dynamic arrest,[42] is predicted to require an aging step where RNAs dynamically sample the surrounding RNAs for intermolecular interactions. The resident RNAs would then form a stable, percolated RNA network upon forming sufficient intermolecular RNA-RNA interactions to reach a local energy minimum, after which G3BP1 scaffolding is no longer required. To test this possibility, we examined the time course by which RNA assemblies became resistant to PK treatment.

We observed that PK-treated *in vitro* co-condensates retain more RNA content following a period of aging before PK treatment when formed with GFP-G3BP1 or untagged G3BP1 (Figures 2A–2C and S3A). Specifically, if G3BP1::RNA co-condensates are immediately treated with PK following assembly, PK-treated *in vitro* co-condensates maintain less than 3% of the RNA signal (Figure 2B). In contrast, the retained RNA content following G3BP1 degradation increases over an hour until ~60%–90% of the RNA signal persists in proteinase-treated samples compared to untreated controls (Figures 2B and 2C). The observed rate of RNA network formation is dependent on Mg^{2+} concentration. At 1 mM Mg^{2+}, stable RNA assemblies are only observed after 24 h of hardening, whereas 10 mM Mg^{2+} promotes network formation rivaling intact granules within an hour (Figures S3B and S3C). We anticipate that the formation of intermolecular RNA-RNA interactions in cells will be promoted by additional components capable of reducing inter-RNA repulsive forces beyond "free" Mg^{2+}, including partially complexed magnesium, polyamines, which can promote RNA condensation,[26] and the positive charges in many RNA-binding domains in SGs, like argine-glycine-glycine (RGG) domains.

The formation of stable RNA networks over time may require the capacity to form base-pairing interactions or other intermolecular RNA-RNA interactions. When co-condensates were formed with mixed-length homopolymers using 10 mM Mg^{2+} RNA assemblies did not persist after PK treatment (Figure 2D),

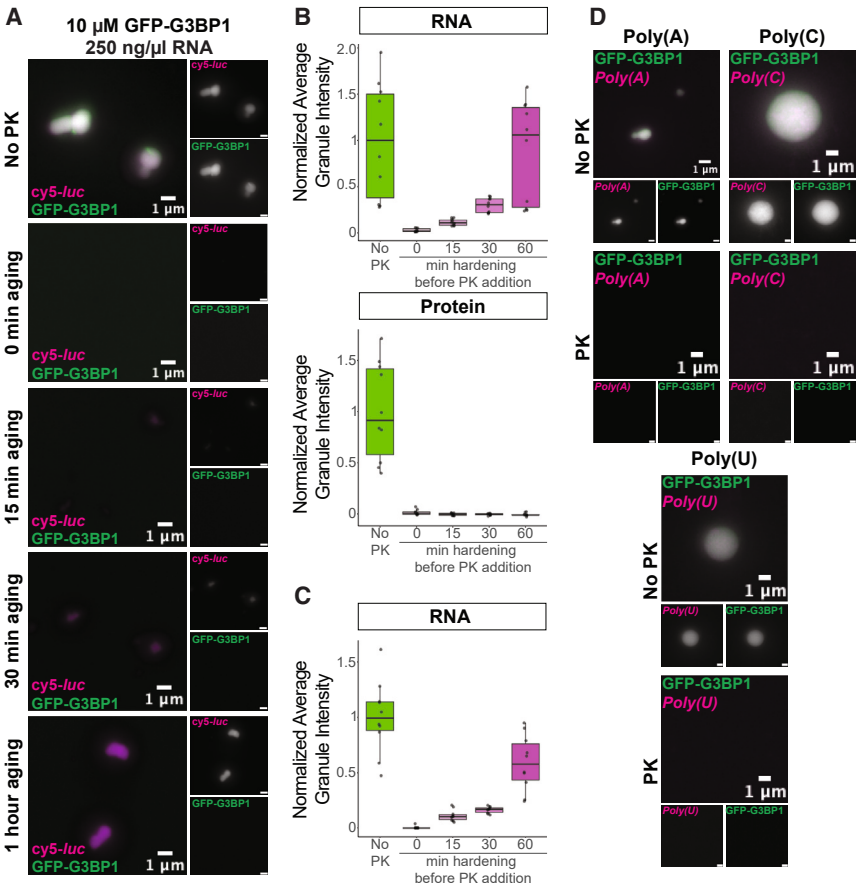

Figure 2. Hardening is required for RNA persistence following G3BP1 degradation

(A) G3BP1::RNA co-condensates were formed using 10 μM GFP-G3BP1 (green), 200 ng/μL total hRNA, and 50 ng/μL cy5-*luciferase* RNA (magenta). Co-condensates were treated with PK (0.1 U/μL) or enzyme buffer (STAR Methods) at the indicated time.

(B) Normalized average RNA (left) or protein (right) intensities in condensates from 10 images from three experiments as performed in (A). All samples were normalized to the average control granule intensity across all images.

(C) G3BP1::RNA co-condensates were formed as in (A) using untagged G3BP1 and quantified as in (B).

(D) G3BP1::RNA co-condensates were formed using 10 μM GFP-G3BP1 (green), 10 ng/μL fluorescently labeled, mixed-length homopolymer, and 100 ng/μL unlabeled homopolymer. Co-condensates were treated with PK at 1 h.

All scale bars represent 1 μm.

See also Figure S3.

except in the case of poly(G), which formed assemblies without G3BP1 (data not shown). The failure of condensates assembled with homopolymer RNAs to persist following removal of G3BP1 implicates intermolecular interactions, including base pairs (see below), in maintaining protease-treated RNA granules.

Together, these results suggest that G3BP1 acts as an RNA condenser by assembling high concentrations of RNA that promote the formation of new intermolecular RNA-RNA interactions in a Mg^{2+}-dependent manner. Following the formation of an arrested RNA network comprising multiple intermolecular interactions, G3BP1 is dispensable for the persistence of RNA-based assemblies.

RNA condensate persistence after G3BP1 degradation requires intermolecular RNA-RNA interactions

The observation that PK-treated RNA granules persist upon degradation of the G3BP1 in co-condensates argues that intermolecular RNA-RNA interactions maintain the resulting RNA assemblies. This model predicts that, following G3BP1 degradation, PK-treated RNA granules should be sensitive to denaturation by treatments that weaken RNA-RNA interactions but not protein-protein or protein-RNA interactions. Given this, we tested the sensitivity of PK-treated *in vitro* co-condensates to RNA or protein denaturants.

Several treatments can denature RNA: EDTA reduces the stability of RNA structure by chelating divalent salts (Mg^{2+}), thus destabilizing the phosphate backbone and reducing charge shielding from water. Disruption of hydrogen bonding with urea or formamide increases the entropy of the system to disfavor RNA folding, and heat treatment enthalpically melts RNA structures.[43–46] Alternatively, proteins can be denatured by high salt concentrations or treatment with aliphatic alcohols such as hexanediol, which denature proteins by competing for electrostatic interactions within folded proteins or weakening the solvation shell and intramolecular hydrogen bonding, respectively.[47–49]

Strikingly, some RNA denaturants completely or near-completely solubilize PK-treated *in vitro* co-condensates (Figures 3A, 3C, and S4A–S4D). As a control, dilution of untreated *in vitro* co-condensates and PK-treated *in vitro* co-condensates in a 25% volume of water for 15 min demonstrates that both co-condensates and PK-treated *in vitro* co-condensates are partially resistant to dilution (~86% and ~52% in untreated and PK-treated, respectively), indicating that any further dissolution following denaturant treatment is due to the denaturant. In contrast, PK-treated *in vitro* co-condensates completely dissolve in 2 M urea or 50 mM EDTA, while identical treatments in undigested co-condensates are insufficient to dissolve the structures (Figures 3A, 3C, and S4A–S4D). Notably, adding RNA denaturants does decrease RNA intensity in intact co-condensates, suggesting that destabilizing the RNA network leads to partial dissolution of co-condensates. Supporting the observation that some RNA denaturation treatments selectively disperse PK-treated *in vitro* co-condensates without completely disrupting untreated co-condensates, heat treatments of 65°C for 10 min or 95°C for 2 min without dilution specifically decrease the intensity of PK-treated *in vitro* co-condensates, reducing their assemblies to 3% and 6% of their pre-treatment intensity, respectively. In

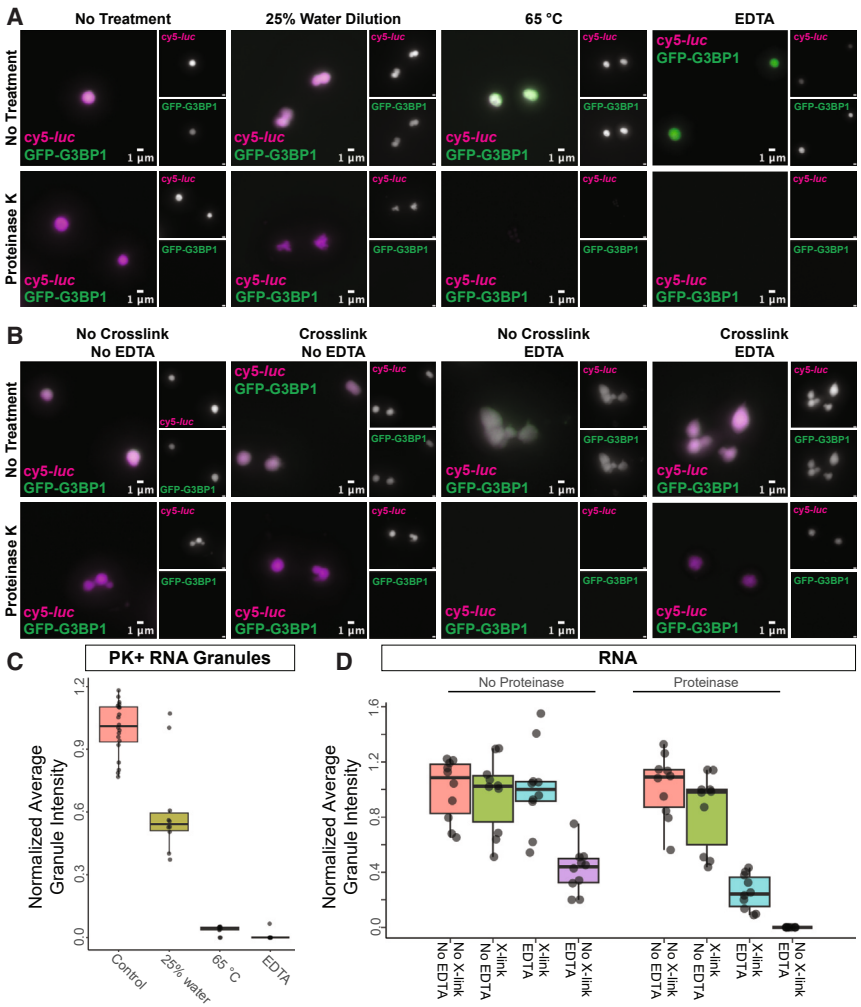

Figure 3. PK-treated RNA granules contain stable RNA-RNA interactions

(A) G3BP1::RNA co-condensates were formed using 10 μM GFP-G3BP1 (green), 200 ng/μL total hRNA, and 50 ng/μL cy5-labeled *luciferase* RNA (magenta) and hardened for 1 h. Co-condensates were treated with equal volumes of either enzyme buffer (STAR Methods) or PK (0.1 U/μL) for 15 min. Samples were diluted or treated with RNA denaturants for 15 min before imaging.

(B) Co-condensates were formed as in (A) with the addition of 10 ng/μL 4′AMT. Following PK treatment or enzyme buffer addition, samples were treated with 10 min 354 nm UV light (columns 2 and 4) or kept in ambient light as controls (columns 1 and 3). Crosslinked and uncrosslinked samples were treated with 50 mM EDTA (columns 3 and 4) or an equal volume of diethyl pyrocarbonate-treated water (columns 1 and 2) for 15 min before imaging.

(C) Normalized average RNA intensities in condensates from 20 images for control samples or 10 for queries collected from 3 experiments as performed in (A). All samples were normalized to the average control granule intensity across all images.

(D) Normalized average RNA intensities in condensates from 10 images from 3 experiments as performed in (B). All samples were normalized to the no proteinase average control granule intensity across all images.

All scale bars represent 1 μm.

See also Figure S4.

contrast, identical treatments have weaker effects on undigested co-condensates (82% and 52% of initial intensity, respectively), indicating that the presence of G3BP1 overcomes the effects of RNA denaturants in co-condensates (Figures 3A, 3C, and S4A–S4D).

In contrast to RNA denaturants, hexanediol or high NaCl, which can disrupt protein structures, do not dissolve PK-treated *in vitro* co-condensates (Figures S4F–S4I). As expected from these treatments, the RNA/protein intensity ratio decreased for all RNA denaturants and increased for protein denaturants for treatments where condensates were present (Figure S4J).

Harsh denaturation conditions, like 4 M urea and 20% formamide, completely dissolved both intact and PK-treated *in vitro* co-condensates (Figures S4A–S4C). The dissolution of even co-condensates suggests that substantial disruption of hydrogen bonding dissolves both RNA and protein structures irrespective of their participation in granule architecture.

The ability of RNA denaturants to dissolve PK-treated *in vitro* co-condensates specifically without disrupting untreated *in vitro* co-condensates suggests that RNA-RNA interactions underlie the stability of RNA granules following the loss of G3BP1.

RNA crosslinking stabilizes PK-treated *in vitro* co-condensates to RNA denaturants

Though RNA denaturation selectively solubilizes PK-treated *in vitro* co-condensates, it remains a formal possibility that protease-resistant fragments of G3BP1 are sufficient to maintain granule organization upon PK treatment. While it is challenging to prove the complete loss of protein from these structures unambiguously, we reasoned that if RNA-RNA interactions significantly contribute to granule structure, RNA-specific crosslinking should render PK-treated *in vitro* co-condensates resistant to treatment with RNA denaturants.

The psoralen derivative 4′ aminomethyltrioxsalen (4′AMT) is a nucleic acid crosslinker that intercalates with stacked nucleic acid bases to form UV-dependent bifunctional adducts near the ends of structured regions. 4′AMT-mediated crosslinks form only when bases are immediately opposed, effectively requiring RNA-RNA duplexes to form crosslinked adducts.[50,51] Thus, if G3BP1 acts as an RNA condenser by catalyzing the formation of new intermolecular RNA-RNA duplexes, 4′AMT crosslinking should stabilize PK-treated *in vitro* co-condensates in the presence of RNA denaturants.

Strikingly, PK-treated *in vitro* co-condensates are made insensitive to RNA denaturants by UV-dependent 4′AMT crosslinking. Specifically, when PK-treated *in vitro* co-condensates were 4′AMT-crosslinked after PK treatment, but before incubation with EDTA, they persisted at levels similar to control conditions

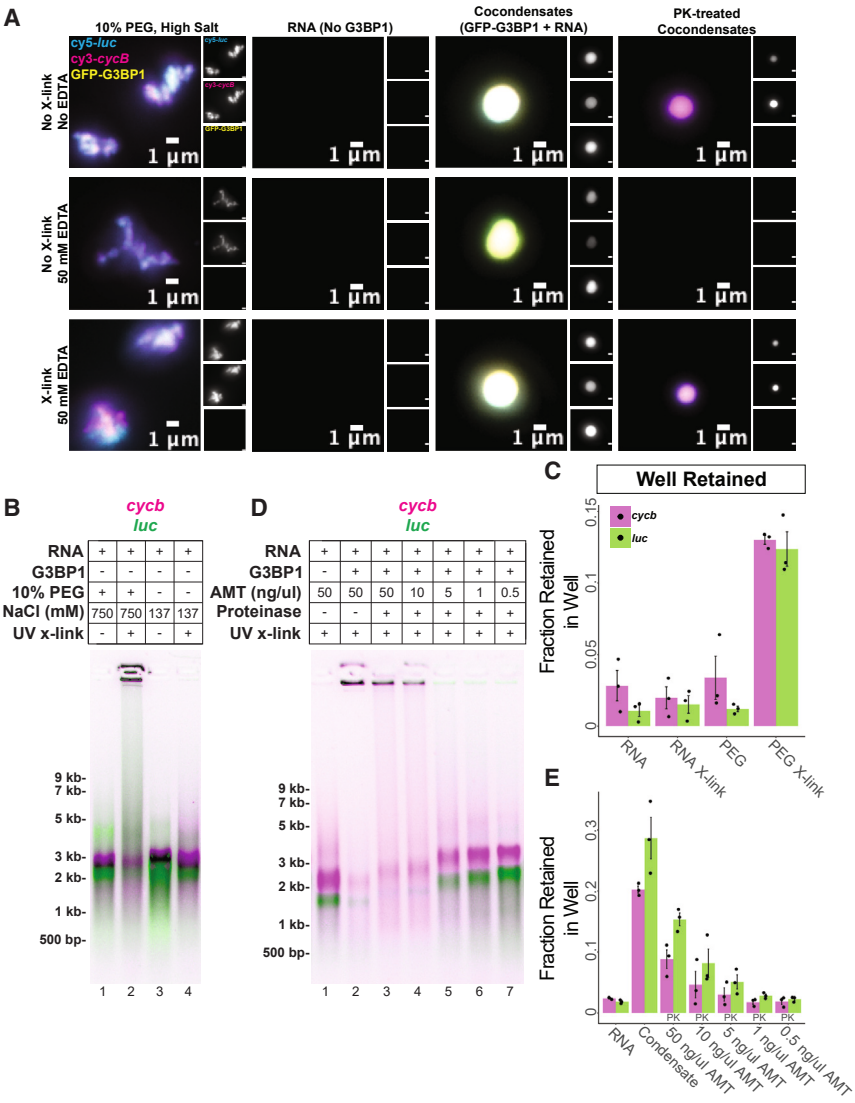

Figure 4. PK-treated RNA granules are high-order structures

(A) Microscopic images of 10% PEG and 750 mM NaCl (left), RNA alone (2nd from left), GFP-G3BP1 co-condensates (2nd from right), or PK-treated *in vitro* co-condensates (right). All images contain 50 ng/μL of cy5-*luciferase* (cyan) and cy3-*cycB* (magenta) RNAs. 10 μM GFP-G3BP1 (yellow) was added to the rightmost 2 lanes. Scale bars represent 1 μm.

(B.) RNA-PEG granules in high-salt buffer (lanes 1 and 2) or RNA alone (lanes 3 and 4) were run on 1% agarose-formaldehyde denaturing gels without (left) or with (right) UV-induced crosslinking. 10 ng/μL 4′AMT was added to each sample. No PK was used in this experiment. Cy3-*cycB* RNA is magenta, and cy5-*luciferase* RNA is green, with black overlay.

(C) The fraction of RNA retained as assemblies in the wells of agarose denaturing gels from (B) was quantified by comparing the total intensity in wells to the total intensity of the entire lane across 3 replicates. Error bars represent the standard deviation.

(D) RNA alone, co-condensates, or PK-treated *in vitro* co-condensates were run on denaturing gels as in (B) with UV-induced crosslinking (lanes 1–3) in the presence of 50 ng/μL 4′AMT. The 4′AMT concentration was titrated down in lanes 4–7 before crosslinking. Cy3-*cycB* RNA is magenta, and cy5-*luciferase* RNA is green, with black overlay.

(E) The fraction of RNA retained in wells was quantified for (D) as in (C) across 3 replicates. Error bars represent the standard deviation.

See also Figure S5.

(Figures 3B, 3D, and S4E). Importantly, the addition of 4′AMT to co-condensate reactions did not affect co-condensates or PK-treated *in vitro* co-condensates with or without exposure to UV treatment (Figures 3B, 3D, and S4E). Furthermore, incorporating 4′AMT without GFP-G3BP1 protein did not cause the formation of microscopic RNA granules with or without exposure to UV, demonstrating that 4′AMT does not independently aggregate RNA (Figure S5A). Thus, the ability for RNA-RNA crosslinking to prevent PK-treated *in vitro* co-condensate dissolution in the presence of RNA denaturants supports the model that RNA-RNA interactions form within the co-condensates and serve as a structural feature stabilizing the RNA assemblies even in the absence of G3BP1.

RNA networks in PK-treated *in vitro* co-condensates consist of stable, high-order structures

The persistence of RNA assemblies after PK digestion of G3BP1 predicts a network of intermolecular RNA-RNA interactions connecting the RNAs within the assemblies. Furthermore, those RNA-RNA interactions can covalently link through 4′AMT crosslinking. This interpretation predicts that PK-treated *in vitro* co-condensates would dissolve and run as individual RNAs on an RNA denaturing gel but, once crosslinked with 4′AMT, would show higher-order assemblies. To resolve specific RNA species in these experiments, we utilized fluorescently labeled, *in vitro* transcribed *luciferase* and *cycB* RNAs. Like co-condensates formed from G3BP1 and total hRNA, reactions containing only these two species of RNA form condensates that are maintained after PK treatment, dissolved with EDTA, and stabilized by 4′AMT crosslinking (Figure 4A).

We first tested how 4′AMT crosslinking affected the mobility of RNAs in condensates by examining RNA-only assemblies without G3BP1, formed in crowding conditions with polyethylene glycol (PEG) and high salt.[26] We observed that PEG-induced RNA assemblies dissolved on formaldehyde gels and ran at their expected sizes for monomeric RNAs (Figures 4B, lane 1, 4C, and S5B). However, when the PEG-induced RNA assemblies are crosslinked with 4′AMT before loading in the gel, ~10%–15% of the RNAs remain in the well when assemblies are formed under high NaCl conditions (Figures 4B, lane 2 and S5B–S5D). This result indicates that crosslinking RNA assemblies covalently links RNAs to stabilize the entire assembly,

reducing gel mobility under denaturing conditions. Notably, even RNA assemblies never exposed to G3BP1 can be specifically crosslinked by 4′AMT, supporting the model that intermolecular RNA-RNA interactions stabilize RNA granules rather than protease-resistant G3BP1 fragments.

Importantly, we also observed that 4′AMT crosslinking of the PK-treated *in vitro* co-condensates led to a shift from singlet species to well retention in a 4′AMT concentration-dependent manner (Figures 4D, lanes 3–7, 4E, and S5E–S5G). As an internal control, G3BP1::RNA co-condensates remain in the well following 4′AMT-directed crosslinking (Figures 4D, lane 2 and S5E), demonstrating that high-order species are also stabilized by crosslinking before protease digestion. Similar high-order PK-treated *in vitro* co-condensate species are observed in the well of denaturing gels when crosslinking *pgc* RNA and *luciferase* (Figures S5H–S5K). These results demonstrate that 4′AMT-induced crosslinking stabilizes high-molecular-weight RNA assemblies that are covalently linked at sites of direct intermolecular RNA-RNA interactions implicating a network of RNA-RNA interactions in the persistence of PK-treated *in vitro* co-condensates.

SGs can persist in cells following disruption of G3BP1 function

An important question is whether G3BP1 promotes intermolecular RNA-RNA interactions in cells during the formation of SGs. If G3BP1 condensation triggers the formation of new RNA-RNA interactions that are stable within SGs, RNA localized to SGs would be predicted to persist following G3BP1 inactivation. However, the persistence of assembled RNAs in SGs would require the inactivation of ATP-dependent SG disassembly factors that displace intermolecular RNA-RNA interactions, like eIF4A.[52] This predicts that once SGs form, if ATP is depleted, then inactivation of G3BP function would lead to persistent SGs. We tested this prediction by treating cells with the G3BP inhibitor a (G3Ia) compound, which binds the G3BP NTFL2 domain inactivating G3BP's ability to promote SG formation or its inactive enantiomer that does not affect SGs.[53]

Using G3Ia, we found that SGs cannot effectively disassemble when ATP is depleted. Specifically, we arsenite stressed cells to induce SGs, with or without subsequent ATP depletion by adding 2-deoxy-D-glucose (2DG) and carbonyl cyanide m-chlorophenylhydrazone (CCCP).[54,55] Strikingly, when cells were both ATP depleted and treated with G3Ia, SGs persisted even when G3BP1 could no longer function as a scaffold (Figures 5A, left and S6). This demonstrates that once SGs are formed, G3BP proteins are not required to maintain the assemblies provided ATP-dependent disassembly systems, including RNA helicases, are inactivated.

We note that in most ATP-depleted cells, G3BP1 remains present in SGs after G3Ia treatment (Figure S6). This likely occurs because the C-terminal G3BP1 RNA recognition motif/RGG domain binds RNA even when the NTF2L dimerization domain is absent and thereby localizes to SGs,[56] which is supported by two observations. First, though SG dynamics decrease upon ATP depletion, G3BP1 still has a fluorescence recovery after photobleaching (FRAP) recovery time of ~35 s,[54] which is an order of magnitude faster than the time scale of this experiment. This suggests that another SG feature, possibly the RNA network, is more stable than G3BP1. Second, in rare cells, we observed *NORAD* and oligo(dT) staining RNA assemblies without G3BP1 signal in ATP-depleted, G3Ia-treated cells (Figure 5A, inset). This argues that G3BP1 is not essential for continued RNA granule persistence under these conditions.

To test if G3BP proteins are only required for the assembly of SGs in cells by another approach, we degraded G3BP1 using a live-cell permeabilization protocol with proteinase treatment.[20] This approach will also degrade SG disassembly factors/RNA decondensers, such as eIF4A, thereby assessing whether RNA-RNA interactions are sufficient to maintain SGs in the absence of both assembly and disassembly factors. Following permeabilization and PK treatment, we examined the persistence/localization of G3BP1 and PABP1 (as a protein marker of SGs) and the localization of *NORAD* and poly(A)+ mRNAs as RNA markers of SGs.

A key result is that the apparent loss of G3BP1 did not alter the assembly of SG RNAs as probed by single-molecule (inexpensive) fluorescence *in situ* hybridization (smFISH/smiFISH). Specifically, permeabilizing cells with PBSTween followed by the addition of PK led to complete loss of GFP signal in GFP-G3BP1 expressing U2OS cells without dispersal of bulk poly(A) RNAs or the resident SG transcript *NORAD* (Figure 5B). Quantification verified that *NORAD* RNA levels and enrichment in granules remained consistent (Figures 5C and 5D). Additionally, line scans of the poly(A) signal showed no apparent difference between PK-treated and untreated cells (Figure 5E). The average intensities of *NORAD* and poly(A) RNA also did not change markedly following protease treatment, though the GFP-G3BP1 signal was completely lost (Figures 5F and 5G). To demonstrate that the loss of protein signal from SGs is not G3BP1 specific, mRuby-PABP1 expressing cells were transfected with EGFP-β-actin,[57] similarly permeabilized, and treated with PK. Upon protein degradation, both EGFP-β-actin and mRuby-PABP1 signals were lost without dissolution of poly(A) RNA granules (Figure S7A). We cannot rule out the persistence of some protease-resistant proteins in these experiments, but the complete loss of fluorescent signal from multiple SG markers supports the susceptibility of SG proteins to PK treatment.

In contrast, treatment with RNase ablated SGs at both the protein and RNA levels in cells where the RNA signal was undetectable, as previously observed[20,58] (Figure S7B). The resilience of SGs to protease treatment and their sensitivity to RNA degradation further support that RNA is an integral structural component of SGs.

RNA components of the nucleoli remain assembled following PK treatment

The persistence of the RNA component of SGs following the loss of SG proteins in cells led us to consider whether other RNP assemblies could contain a stable RNA network. Previous work demonstrated that ongoing transcription is essential for the organization of the nucleolus and that induction of RNase L within the nucleus causes dissolution of the nucleolus.[59,60] These observations show that RNA is essential for the formation and persistence of the nucleolus and raises the potential for RNA-RNA interactions in forming this organelle. To determine whether nucleolar RNAs form stable networks that persist in the absence

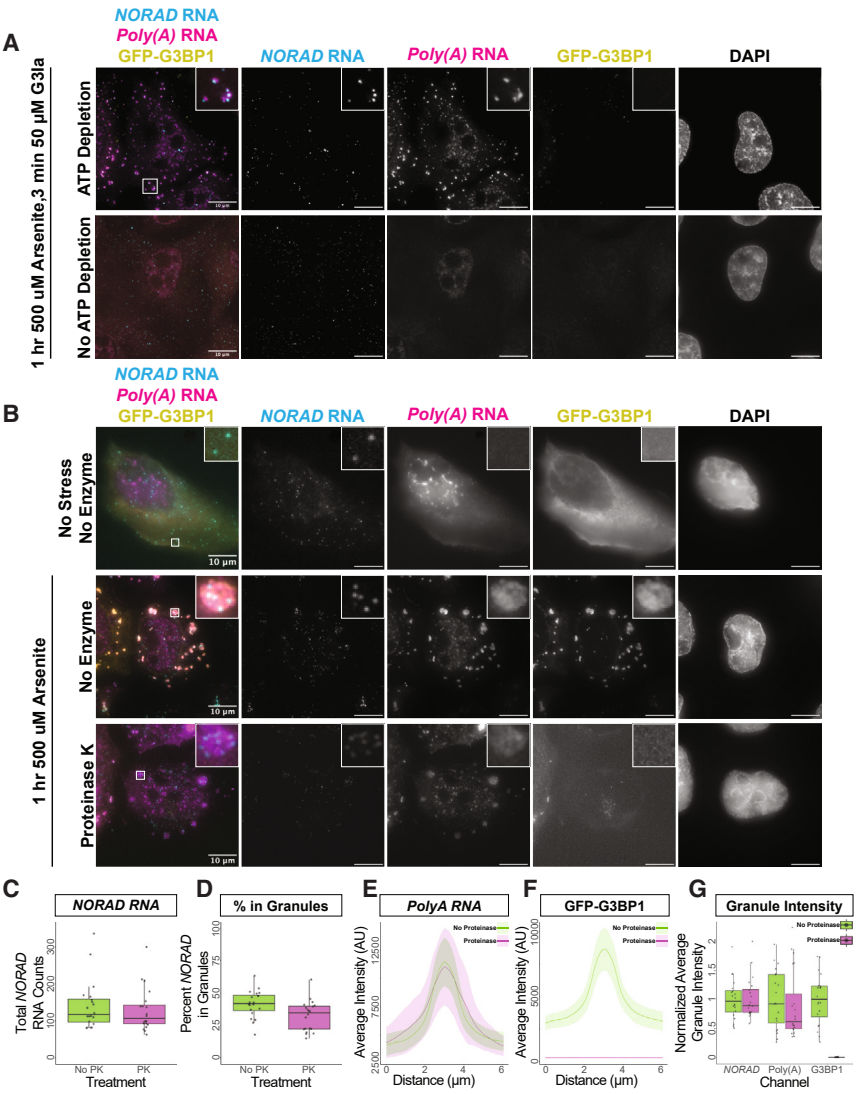

Figure 5. Stress granule RNAs persist *in vivo* following degradation of G3BP

(A) U2OS cells stably expressing GFP-G3BP1 were treated with stress (500 µM sodium arsenite) for 1 h and G3Ia (50 µM) for 3 min prior to fixation. In ATP-depleted cells, media was supplemented with CCCP (100 µM) and 2DG (200 mM) 30 min prior to fixation. smFISH was performed using cy3-oligo(dT) and Quasar 670-*NORAD* RNA probes.

(B) GFP-G3BP1 cells were treated with arsenite for 1 h or left as controls before permeabilization with PBS containing 0.2% Tween 20 for 10 min. Cells were then treated with either PBS alone or PBS containing 0.02 U/µL PK for 3 min. Following treatment, smFISH was performed using cy3-oligo(dT) and Quasar 670-*NORAD* RNA probes.

(C) *NORAD* RNA spots were counted in arsenite-exposed cells with or without proteinase treatment using FISHquant. Error bars represent standard deviation.

(D) *NORAD* RNA spots were compared to masks of cytoplasmic *poly(A)* staining in arsenite-exposed cells with or without proteinase treatment to determine the retention of *NORAD* RNA within granules. Error bars represent standard deviation.

(E) Line scans were taken across 20 *poly(A)* granules in arsenite-exposed cells with or without proteinase treatment. Line plots show the average intensity of *poly(A)* centered on the brightest point. Ribbon shows 95% confidence intervals. No proteinase treatment is shown in green, and PK-treated samples are in magenta.

(F) Line scans were taken across 20 GFP-G3BP1 granules as for *poly(A)* in (E). No proteinase treatment is shown in green, and PK-treated samples are in magenta.

(G) The normalized average intensity of *NORAD* RNA spots, *poly(A)* assemblies, and GFP-G3BP1 was quantified using FISHquant-identified spots (*NORAD*) or *poly(A)* masks (*poly(A)* and G3BP1) over 20 cells from 3 replicates. Error bars represent standard deviation.

All scale bars represent 10 µm.

See also Figures S6 and S7.

of nucleolar proteins, we examined nucleolar RNA and protein markers following PK treatment of permeabilized cells.

Strikingly, we observed that the 47S 5′ external transcribed spacer (5′ETS) RNA component of nucleoli remained concentrated even after degradation of nucleolar proteins. Specifically, we observed that PK infusion degraded the signal of the nucleolar marker NPM1,[61] but nucleoli persisted as visualized by the 47S 5′ETS RNA (Figures 6A–6C). The low DNA density within nucleoli is also preserved following PK treatment when visualized by DAPI staining.[62] The persistence of these nucleolar markers is consistent with RNA alone being sufficient to maintain gross nucleolar morphology following the loss of nucleolar proteins.

Interestingly, the small nucleolar RNA (snoRNA) *snoRD3A* loses much of its nucleolar enrichment following proteinase treatment (Figures 6A and 6D). The dispersal of *snoRD3A* suggests that highly structured RNAs like snoRNAs may not have sufficient accessible regions to form stable intermolecular interactions within RNA assemblies but rather require protein-directed recruitment and retention. Additionally, there may be a minimum size requirement for RNAs to form stable networks in the absence of scaffolding proteins, which is consistent with the multivalent nature of condensate assembly and the length dependence of RNA condensation.[26,28] Furthermore, the dispersal of *snoRD3A* demonstrates that PK treatment is sufficient to disrupt the localization of some condensate RNAs.

In conjunction with the finding that the RNA component of SGs persists after SG protein degradation, these results suggest that protein-directed RNA condensation to form a stable RNA network may be a common feature of RNP organelles.

DISCUSSION

G3BP1 functions as an RNA condenser

We provide several observations that G3BP1 promotes SG formation by first promoting RNA-G3BP1 condensation, and then the resulting high local concentration of RNA leads to the formation of intermolecular RNA-RNA interactions that stabilize

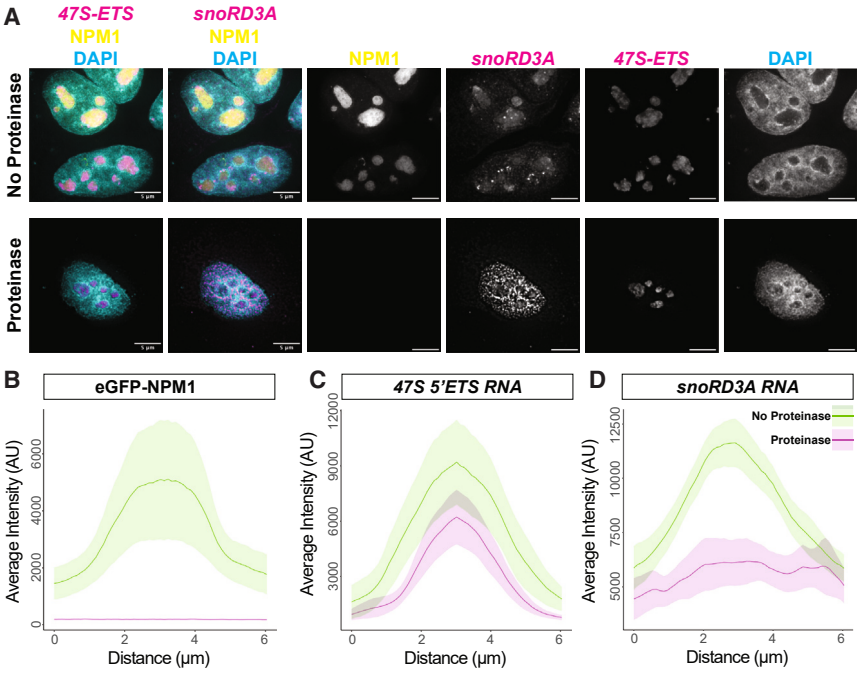

Figure 6. The 47S-ETS retains nucleolar localization following nucleolar protein degradation

(A) U2OS cells transiently transfected with EGFP-NPM1 (yellow) were permeabilized in PBS containing 0.2% Tween 20 for 10 min. Cells were then treated with PBS alone or PBS containing 0.02 U/μL PK for 3 min. Following treatment, smFISH was performed, probing for the *47S-ETS1* RNA (magenta, left) using a smiFISH probe set designed using sequences from Yao et al.[59] as the primary probe-binding sequence and an ATTO550 FLAPY secondary probe and *snoRD3A* RNA (magenta, right) with an Alexa Fluor 647-labeled oligo. Scale bars represent 5 μm.

(B–D) EGFP-NPM1 (B), 47S 5′ETS1 (C), and *snoRD3A* (D) line scans were taken across 20 nucleoli in cells with or without proteinase treatment. Line plots show the average intensity of their respective signal centered on the brightest point corresponding to the *47S 5′ETS1* signal. Ribbon shows 95% confidence intervals. No proteinase treatment is shown in green, and PK-treated samples are in magenta.

the assembly. First, G3BP1::RNA co-condensates formed *in vitro* harden over time to become stable even following the degradation of G3BP1 (Figures 1 and 2). Second, the RNA granules remaining after G3BP1 removal are sensitive to RNA denaturants but are protected from denaturation by crosslinking across RNA duplexes (Figure 3). Third, RNA duplex crosslinking leads to high-order assemblies of RNA that are incapable of penetrating denaturing agarose gels (Figure 4). Finally, rapid inhibition or proteolysis of G3BP1 and the bulk cellular proteome in permeabilized cells leaves stable assemblies of SG RNAs intact, consistent with our *in vitro* observations (Figure 5). Together, these results implicate a role for G3BP1 in SG assembly by creating a high local concentration of RNA, which can subsequently sample diverse RNA-RNA interactions to find local energy minima and form stable RNA networks.

The ability of G3BP1 to promote intermolecular RNA-RNA interactions provides a molecular explanation for UV-induced SGs activating PKR.[63] When splicing is inhibited and pre-mRNAs rich in Alu elements are released to the cytosol during mitosis, they are condensed into "DHX9-SGs," which form dsRNA in a G3BP1-dependent manner activating PKR. This demonstrates how G3BP1 can promote intermolecular RNA interactions and highlights how such an activity might explain some of G3BP's antiviral roles.[16,64]

Other multivalent RNA-binding proteins capable of condensing RNA may also promote intermolecular RNA-RNA interactions to form stable networks. For example, we observed that MEG-3, an RNP granule assembly factor for P-granules in *C. elegans*, promotes the formation of RNA condensates persisting after PK treatment (Figure 1). Similarly, the localization-body forming PTBP3 protein in *Xenopus* oocytes drives RNA condensation *in vitro*, forming assemblies resistant to PK.[65] We predict that the high local concentration of RNAs within RNP granules will make this a general feature of RNP granules and RNA-containing condensates.

Stable RNA granules evoke a need for an RNA chaperone network

The ability of condensed RNA to form stable crosslinked RNA assemblies creates a biological need to limit or disassemble such stable, potentially detrimental RNA aggregates. Indeed, mammalian cells contain monovalent RNA-binding proteins and DEAD-box RNA helicases to compete with, or disassemble, intermolecular RNA-RNA interactions and thereby limit RNA aggregation.[32,66] One anticipates that within an RNP granule, there is a dynamic equilibrium between the formation of new intermolecular RNA-RNA interactions and their dissociation by "RNA decondensers." Thus, to maintain the dynamics of SGs, active ATP-dependent processes are required to limit intermolecular RNA-RNA interactions. Indeed, two observations highlight that an RNA decondenser network can dissemble SG when G3BP1 is inhibited in cells. First, when we simultaneously inactivate G3BP1 and other proteins by PK addition, we observe that the RNA in SGs persists in an assembled state. Second, we demonstrate that G3BP1 dimer disruption leads to the persistence of SGs, but only when ATP is depleted (thereby inactivating ATP-dependent RNA "decondensers"). These observations suggest that G3BP1 can promote new intermolecular RNA-RNA interactions, and cells utilize ATP-dependent mechanisms (including eIF4A) to limit such RNA-RNA interactions and maintain a fluid state of SG dynamics.

RNP granule condensates are dense networks that promote RNA-RNA interactions

Several observations support the view that other RNP granules also contain a dense, stable network of RNA-RNA interactions that have been previously unrecognized. First, we observe that

SG RNAs are stable in the absence of SG proteins in the cell. Second, RNAs with extended disordered regions are suggested to form large and immobile reticulated networks *in vivo*.[4,34] Third, RNAs within SGs maintain a constant relative position with one another,[37] consistent with multiple interactions locking the mRNAs into position. Together, these observations demonstrate that many RNP granules, in addition to SGs, may contain dense networks of RNA-RNA interactions.

The condensate environment within RNP granules may influence the assembly of these dense RNA-RNA interaction networks. For instance, some experimental conditions have demonstrated that condensation can promote the folding of structured RNAs.[27,67,68] Furthermore, it has been demonstrated that protein low-complexity domains modulate the aging properties of RNAs within condensates.[42] This low-complexity domain-dependent modulation of aging is particularly interesting in the context of recent work demonstrating that condensed RNAs are balancing an enthalpic line between reversibility and dynamic arrest dependent on percolation temperature and lower critical solution temperature.[27] Given these results, the role of RNA condensing proteins may not be scaffolding condensates per se but instead to raise the percolation temperature of the constituent RNAs and facilitate the assembly of stable RNA scaffolds.

How RNA-binding proteins affect the condensation of RNA will be affected by multiple features, including the kinetic rates of RBP-RNA and RNA-RNA interactions, the time before analysis, the length of the RNAs, and the relative thermodynamic stability of RBP-RNA and RNA-RNA interactions. For example, G3BP1 limits the initial formation of highly stable G-quadraplexes of poly(G) homopolymers, which may be explained by G3BP1-RNA interaction being kinetically favored over intermolecular G-quadraplex interactions, but with extended time the more stable RNA-RNA interactions form.[22] Similarly, RNA-protein condensates with short RNAs may be dominated by protein interactions since short RNAs will be limited in their ability to form additional intermolecular RNA-RNA interactions.[69]

Are condensate chaperones mistaken for integral condensate scaffolding proteins?

Our observation that G3BP1 can be dispensable for the persistence of RNA granules *in vitro* and *in vivo* suggests that G3BP1 is not a scaffold of SGs per se but rather an assembly factor used to form new RNA-RNA interactions. In this role, we suggest that G3BP1 functions as an RNA condenser, a protein that first creates a high local RNA concentration, which then forms a dense network of RNA-RNA interactions, stabilizing the assembly. We anticipate that other key factors for condensate formation, perhaps including MEG-3, will similarly function as such condensate chaperones. Condensate chaperones would be essential for the assembly of condensates but would be highly dynamic within the condensate and dispensable once the assembly had formed a percolated network of stabilizing interactions. Indeed, it remains possible that in some cases, the recognized "scaffolding" molecules of well-studied condensates may rather be condensate chaperones.

An unanswered question is whether any multivalent RNA-binding protein would function as an RNA condenser. To function efficiently, an RNA condenser should have two critical features. First, it should bind RNAs in a manner that minimizes the ΔG^{act} for the formation of new intermolecular RNA-RNA interactions (Figure 7). Such a mechanism could be achieved by either binding RNA in a strained state such that the initial bound state is of higher energy or by having features that stabilize the transition state, such as binding unfolded single-stranded regions. A second critical feature will be to have an average residence time on the RNA longer than the time scale of transient unfolding for local RNA secondary structures. Given these features, we hypothesize that the ability of multivalent RNA-binding proteins to condense RNA will vary significantly.

Limitations of the study

This work has two limitations. First, while our data suggest RNA-RNA interactions form within SGs in cells to stabilize those structures, we cannot unequivocally demonstrate that the persistence of RNA-enriched SGs following inactivation or degradation is due to RNA-RNA interactions that were present prior to intervention. It remains a formal possibility that the persistence of SG RNA assemblies in cells may be a consequence of protein degradation or ATP depletion, with intermolecular RNA-RNA interactions normally limited by a robust RNA decondenser network.

A second limitation of this work is that we have not yet mapped the specific intermolecular RNA-RNA interactions that can form in SGs and/or other RNP granules. Given this, it is hard to predict the relative importance of Watson-Crick duplexes or other non-Watson-Crick interactions such as G-quadruplexes or triple helices. It also remains unclear if specific conserved sequence motifs promote intermolecular RNA-RNA interactions or if there is a random assortment of short multivalent interactions between the long RNAs within SGs.

RESOURCE AVAILABILITY

Lead contact

For additional information and resource requests, contact Roy Parker (roy.parker@colorado.edu).

Materials availability

No new reagents were generated in this study.

Data and code availability

- Due to file size constraints, data are available upon request.
- All scripts used to process data are available at Zenodo: https://doi.org/10.5281/zenodo.14027059 at the date of publication.
- Any additional information required to reanalyze the data reported in this paper is available from the lead contact upon request.

ACKNOWLEDGMENTS

We thank the Parker lab, Paul Taylor, and Olke Uhlenbeck for discussions. We thank the University of Colorado BioFrontiers Institute Cell Culture Facility, Advanced Light Microscopy Core Facility, and Shared Instruments Pool Core Facility (RRID: SCR_018988, RRID: SCR_018302, and RRID: SCR_018986) as well as Paul Taylor for providing reagents, instruments, and advice. This work was funded by the Damon Runyon Cancer Research Foundation Postdoctoral Fellowship award, DRG 2471-22 (D.M.P.) and the Howard Hughes Medical Institute.

CellPress
OPEN ACCESS

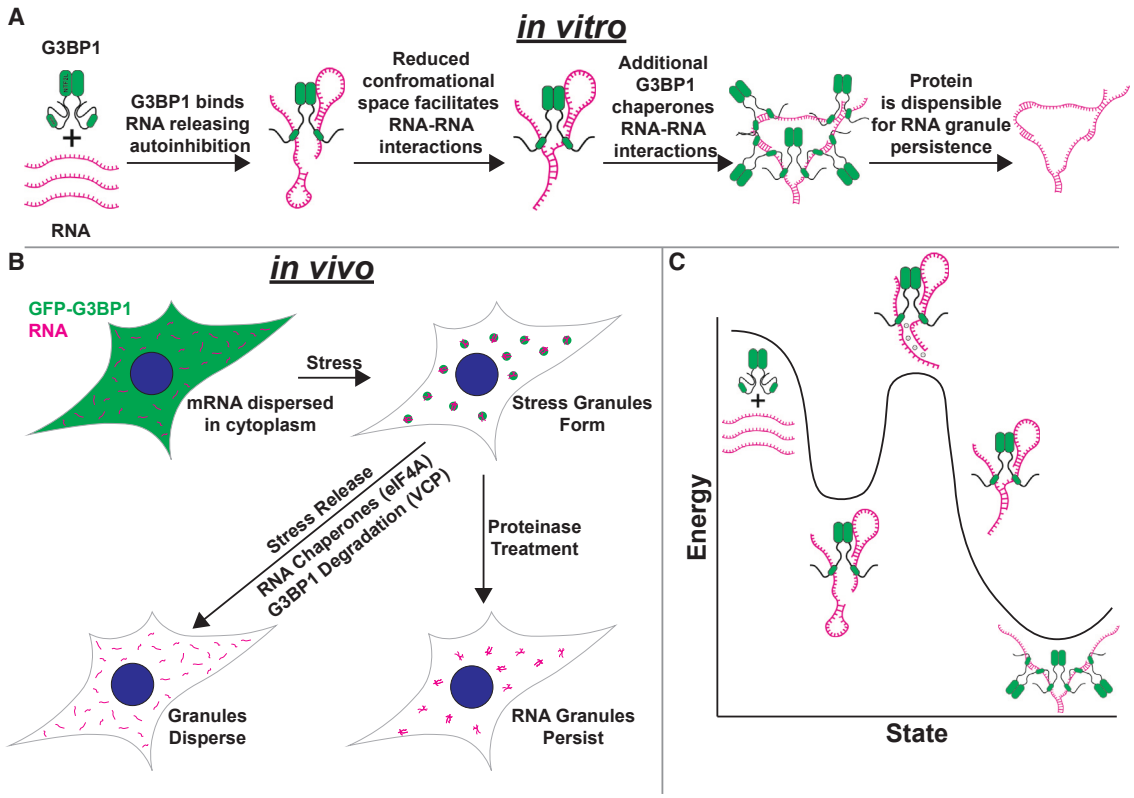

Figure 7. A model for G3BP1's function as an RNA condenser

(A and B) A model mechanism for G3BP1's role as an RNA condenser *in vitro* (A) and *in vivo* (B).

(C) An energy diagram illustrating how G3BP1 may overcome the repulsive intermolecular forces acting on RNAs to facilitate RNA condensation.

AUTHOR CONTRIBUTIONS

Conceptualization, D.M.P., D.T., and R.P.; data curation, D.M.P.; formal analysis, D.M.P.; funding acquisition, D.M.P. and R.P.; writing – original draft, D.M.P. and R.P.; writing – review and editing, D.M.P., D.T., and R.P.

DECLARATION OF INTERESTS

The authors declare no competing interests.

STAR★METHODS

Detailed methods are provided in the online version of this paper and include the following:

- KEY RESOURCES TABLE
- EXPERIMENTAL MODEL AND STUDY PARTICIPANT DETAILS
  - Bacterial cell culture
  - Human cell culture, transfection, and oxidative stress
- METHOD DETAILS
  - G3BP1 protein purification
  - MEG-3 protein purification
  - *In vitro* transcription
  - Homopolymer labeling
  - Total RNA extraction
  - *In vitro* condensate formation
  - Enzyme treatment of co-condensates
  - SDS-PAGE
  - Condensate dissolution
  - *In vitro* crosslinking
  - Denaturing agarose gel electrophoresis
  - ATP depletion with G3la treatment
  - Permeabilization and intracellular enzyme treatment
  - Single-molecule (inexpensive) RNA FISH
  - Microscopy
- QUANTIFICATION AND STATISTICAL ANALYSIS
  - Quantification of *in vitro* granule intensity
  - Pelleting of *in vitro* co-condensates
  - Quantification of RNA denaturing gels
  - Analysis of cellular RNA counts, localization, and intensity
  - Line scans

SUPPLEMENTAL INFORMATION

Supplemental information can be found online at https://doi.org/10.1016/j.molcel.2024.11.012.

Received: March 6, 2024
Revised: August 23, 2024
Accepted: November 8, 2024
Published: December 4, 2024

REFERENCES

1. Banani, S.F., Lee, H.O., Hyman, A.A., and Rosen, M.K. (2017). Biomolecular condensates: organizers of cellular biochemistry. Nat. Rev. Mol. Cell Biol. *18*, 285–298. https://doi.org/10.1038/nrm.2017.7.

2. Shin, Y., and Brangwynne, C.P. (2017). Liquid phase condensation in cell physiology and disease. Science *357*, eaaf4382. https://doi.org/10.1126/science.aaf4382.

3. Parker, D.M., Winkenbach, L.P., and Osborne Nishimura, E.O. (2022). It's Just a Phase: Exploring the Relationship Between mRNA, Biomolecular Condensates, and Translational Control. Front. Genet. *13*, 931220. https://doi.org/10.3389/fgene.2022.931220.

4. Ma, W., and Mayr, C. (2018). A Membraneless Organelle Associated with the Endoplasmic Reticulum Enables 3′UTR-Mediated Protein-Protein Interactions. Cell *175*, 1492–1506.e19. https://doi.org/10.1016/j.cell.2018.10.007.

5. Huizar, R.L., Lee, C., Boulgakov, A.A., Horani, A., Tu, F., Marcotte, E.M., Brody, S.L., and Wallingford, J.B. (2018). A liquid-like organelle at the root of motile ciliopathy. eLife *7*, e38497. https://doi.org/10.7554/eLife.38497.

6. Hubstenberger, A., Courel, M., Bénard, M., Souquere, S., Ernoult-Lange, M., Chouaib, R., Yi, Z., Morlot, J.-B., Munier, A., Fradet, M., et al. (2017). P-Body Purification Reveals the Condensation of Repressed mRNA Regulons. Mol. Cell *68*, 144–157.e5. https://doi.org/10.1016/j.molcel.2017.09.003.

7. Voronina, E., Seydoux, G., Sassone-Corsi, P., and Nagamori, I. (2011). RNA granules in germ cells. Cold Spring Harb. Perspect. Biol. *3*, a002774. https://doi.org/10.1101/cshperspect.a002774.

8. Yu, X., Li, B., Jang, G.-J., Jiang, S., Jiang, D., Jang, J.-C., Wu, S.-H., Shan, L., and He, P. (2019). Orchestration of Processing Body Dynamics and mRNA Decay in Arabidopsis Immunity. Cell Rep. *28*, 2194–2205.e6. https://doi.org/10.1016/j.celrep.2019.07.054.

9. Zheng, Z.-Q., Wang, S.-Y., Xu, Z.-S., Fu, Y.-Z., and Wang, Y.-Y. (2021). SARS-CoV-2 nucleocapsid protein impairs stress granule formation to promote viral replication. Cell Discov. *7*, 38. https://doi.org/10.1038/s41421-021-00275-0.

10. Xia, J., Chen, X., Xu, F., Wang, Y., Shi, Y., Li, Y., He, J., and Zhang, P. (2015). Dengue virus infection induces formation of G3BP1 granules in human lung epithelial cells. Arch. Virol. *160*, 2991–2999. https://doi.org/10.1007/s00705-015-2578-9.

11. Fan, A.C., and Leung, A.K.L. (2016). RNA Granules and Diseases: A Case Study of Stress Granules in ALS and FTLD. Adv. Exp. Med. Biol. *907*, 263–296. https://doi.org/10.1007/978-3-319-29073-7_11.

12. Zhang, K., Daigle, J.G., Cunningham, K.M., Coyne, A.N., Ruan, K., Grima, J.C., Bowen, K.E., Wadhwa, H., Yang, P., Rigo, F., et al. (2018). Stress Granule Assembly Disrupts Nucleocytoplasmic Transport. Cell *173*, 958–971.e17. https://doi.org/10.1016/j.cell.2018.03.025.

13. Anderson, P., Kedersha, N., and Ivanov, P. (2015). Stress granules, P-bodies and cancer. Biochim. Biophys. Acta *1849*, 861–870. https://doi.org/10.1016/j.bbagrm.2014.11.009.

14. Lavalée, M., Curdy, N., Laurent, C., Fournié, J.-J., and Franchini, D.-M. (2021). Cancer cell adaptability: turning ribonucleoprotein granules into targets. Trends Cancer *7*, 902–915. https://doi.org/10.1016/j.trecan.2021.05.006.

15. Song, M.-S., and Grabocka, E. (2020). Stress Granules in Cancer. In Organelles in Disease. Reviews of Physiology, Biochemistry and Pharmacology, *185* (Springer), pp. 25–52. https://doi.org/10.1007/112_2020_37.

16. Burke, J.M., Ratnayake, O.C., Watkins, J.M., Perera, R., and Parker, R. (2024). G3BP1-dependent condensation of translationally inactive viral RNAs antagonizes infection. Sci. Adv. *10*, eadk8152. https://doi.org/10.1126/sciadv.adk8152.

17. Ripin, N., and Parker, R. (2023). Formation, function, and pathology of RNP granules. Cell *186*, 4737–4756. https://doi.org/10.1016/j.cell.2023.09.006.

18. Hofmann, S., Kedersha, N., Anderson, P., and Ivanov, P. (2021). Molecular mechanisms of stress granule assembly and disassembly. Biochim. Biophys. Acta Mol. Cell Res. *1868*, 118876. https://doi.org/10.1016/j.bbamcr.2020.118876.

19. Campos-Melo, D., Hawley, Z.C.E., Droppelmann, C.A., and Strong, M.J. (2021). The Integral Role of RNA in Stress Granule Formation and Function. Front. Cell Dev. Biol. *9*, 621779. https://doi.org/10.3389/fcell.2021.621779.

20. Yang, P., Mathieu, C., Kolaitis, R.-M., Zhang, P., Messing, J., Yurtsever, U., Yang, Z., Wu, J., Li, Y., Pan, Q., et al. (2020). G3BP1 Is a Tunable Switch that Triggers Phase Separation to Assemble Stress Granules. Cell *181*, 325–345.e28. https://doi.org/10.1016/j.cell.2020.03.046.

21. Sanders, D.W., Kedersha, N., Lee, D.S.W., Strom, A.R., Drake, V., Riback, J.A., Bracha, D., Eeftens, J.M., Iwanicki, A., Wang, A., et al. (2020). Competing Protein-RNA Interaction Networks Control Multiphase Intracellular Organization. Cell *181*, 306–324.e28. https://doi.org/10.1016/j.cell.2020.03.050.

22. Guillén-Boixet, J., Kopach, A., Holehouse, A.S., Wittmann, S., Jahnel, M., Schlüßler, R., Kim, K., Trussina, I.R.E.A., Wang, J., Mateju, D., et al. (2020). RNA-Induced Conformational Switching and Clustering of G3BP Drive Stress Granule Assembly by Condensation. Cell *181*, 346–361.e17. https://doi.org/10.1016/j.cell.2020.03.049.

23. Kedersha, N., Panas, M.D., Achorn, C.A., Lyons, S., Tisdale, S., Hickman, T., Thomas, M., Lieberman, J., McInerney, G.M., Ivanov, P., et al. (2016). G3BP–Caprin1–USP10 complexes mediate stress granule condensation and associate with 40S subunits. J. Cell Biol. *212*, 845–860. https://doi.org/10.1083/jcb.201508028.

24. Tourrière, H., Chebli, K., Zekri, L., Courselaud, B., Blanchard, J.M., Bertrand, E., and Tazi, J. (2003). The RasGAP-associated endoribonuclease G3BP assembles stress granules. J. Cell Biol. *160*, 823–831. https://doi.org/10.1083/jcb.200212128.

25. Kedersha, N.L., and Anderson, P. (2002). Stress granules: sites of mRNA triage that regulate mRNA stability and translatability. Biochem. Soc. Trans. *30*, 963–969. https://doi.org/10.1042/bst0300963.

26. Van Treeck, B., Protter, D.S.W., Matheny, T., Khong, A., Link, C.D., and Parker, R. (2018). RNA self-assembly contributes to stress granule formation and defining the stress granule transcriptome. Proc. Natl. Acad. Sci. USA *115*, 2734–2739. https://doi.org/10.1073/pnas.1800038115.

27. Wadsworth, G.M., Zahurancik, W.J., Zeng, X., Pullara, P., Lai, L.B., Sidharthan, V., Pappu, R.V., Gopalan, V., and Banerjee, P.R. (2023). RNAs undergo phase transitions with lower critical solution temperatures. Nat. Chem. *15*, 1693–1704. https://doi.org/10.1038/s41557-023-01353-4.

28. Banani, S.F., Rice, A.M., Peeples, W.B., Lin, Y., Jain, S., Parker, R., and Rosen, M.K. (2016). Compositional Control of Phase-Separated Cellular Bodies. Cell *166*, 651–663. https://doi.org/10.1016/j.cell.2016.06.010.

29. Lee, C.S., Putnam, A., Lu, T., He, S., Ouyang, J.P.T., and Seydoux, G. (2020). Recruitment of mRNAs to P granules by condensation with intrinsically-disordered proteins. eLife *9*, 1–31. https://doi.org/10.7554/eLife.52896.

30. Dundr, M., Hebert, M.D., Karpova, T.S., Stanek, D., Xu, H., Shpargel, K.B., Meier, U.T., Neugebauer, K.M., Matera, A.G., and Misteli, T. (2004). In vivo kinetics of Cajal body components. J. Cell Biol. *164*, 831–842. https://doi.org/10.1083/jcb.200311121.

31. Kedersha, N., Stoecklin, G., Ayodele, M., Yacono, P., Lykke-Andersen, J., Fritzler, M.J., Scheuner, D., Kaufman, R.J., Golan, D.E., and Anderson, P. (2005). Stress granules and processing bodies are dynamically linked sites of mRNP remodeling. J. Cell Biol. *169*, 871–884. https://doi.org/10.1083/jcb.200502088.

32. Tauber, D., Tauber, G., and Parker, R. (2020). Mechanisms and Regulation of RNA Condensation in RNP Granule Formation. Trends Biochem. Sci. *45*, 764–778. https://doi.org/10.1016/j.tibs.2020.05.002.

33. Ranganathan, S., and Shakhnovich, E.I. (2020). Dynamic metastable long-living droplets formed by sticker-spacer proteins. eLife *9*, e56159. https://doi.org/10.7554/eLife.56159.

34. Ma, W., Zhen, G., Xie, W., and Mayr, C. (2021). In vivo reconstitution finds multivalent RNA–RNA interactions as drivers of mesh-like condensates. eLife *10*, e64252. https://doi.org/10.7554/eLife.64252.

35. Cheng, S., Altmeppen, G., So, C., Welp, L.M., Penir, S., Ruhwedel, T., Menelaou, K., Harasimov, K., Stützer, A., Blayney, M., et al. (2022). Mammalian oocytes store mRNAs in a mitochondria-associated membraneless compartment. Science *378*, eabq4835. https://doi.org/10.1126/science.abq4835.

36. Erkamp, N.A., Sneideris, T., Ausserwöger, H., Qian, D., Qamar, S., Nixon-Abell, J., St George-Hyslop, P.S., Schmit, J.D., Weitz, D.A., and Knowles, T.P.J. (2023). Spatially non-uniform condensates emerge from dynamically arrested phase separation. Nat. Commun. *14*, 684. https://doi.org/10.1038/s41467-023-36059-1.

37. Moon, S.L., Morisaki, T., Khong, A., Lyon, K., Parker, R., and Stasevich, T.J. (2019). Multicolour single-molecule tracking of mRNA interactions with RNP granules. Nat. Cell Biol. *21*, 162–168. https://doi.org/10.1038/s41556-018-0263-4.

38. Putnam, A., Cassani, M., Smith, J., and Seydoux, G. (2019). A gel phase promotes condensation of liquid P granules in Caenorhabditis elegans embryos. Nat. Struct. Mol. Biol. *26*, 220–226. https://doi.org/10.1038/s41594-019-0193-2.

39. Brangwynne, C.P., Eckmann, C.R., Courson, D.S., Rybarska, A., Hoege, C., Gharakhani, J., Jülicher, F., and Hyman, A.A. (2009). Germline P Granules Are Liquid Droplets That Localize by Controlled Dissolution/Condensation. Science *324*, 1729–1732. https://doi.org/10.1126/science.1172046.

40. Hanazawa, M., Yonetani, M., and Sugimoto, A. (2011). PGL proteins self associate and bind RNPs to mediate germ granule assembly in C. elegans. J. Cell Biol. *192*, 929–937. https://doi.org/10.1083/jcb.201010106.

41. Schmidt, H., Putnam, A., Rasoloson, D., and Seydoux, G. (2021). Protein-based condensation mechanisms drive the assembly of RNA-rich P granules. eLife *10*, e63698. https://doi.org/10.7554/eLife.63698.

42. Linsenmeier, M., Hondele, M., Grigolato, F., Secchi, E., Weis, K., and Arosio, P. (2022). Dynamic arrest and aging of biomolecular condensates are modulated by low-complexity domains, RNA and biochemical activity. Nat. Commun. *13*, 3030. https://doi.org/10.1038/s41467-022-30521-2.

43. Yamagami, R., Sieg, J.P., and Bevilacqua, P.C. (2021). Functional Roles of Chelated Magnesium Ions in RNA Folding and Function. Biochemistry *60*, 2374–2386. https://doi.org/10.1021/acs.biochem.1c00012.

44. Shelton, V.M., Sosnick, T.R., and Pan, T. (1999). Applicability of Urea in the Thermodynamic Analysis of Secondary and Tertiary RNA Folding. Biochemistry *38*, 16831–16839. https://doi.org/10.1021/bi991699s.

45. Lambert, D., and Draper, D.E. (2012). Denaturation of RNA Secondary and Tertiary Structure by Urea: Simple Unfolded State Models and Free Energy Parameters Account for Measured m-Values. Biochemistry *51*, 9014–9026. https://doi.org/10.1021/bi301103j.

46. Blake, R.D., and Delcourt, S.G. (1996). Thermodynamic Effects of Formamide on DNA Stability. Nucleic Acids Res. *24*, 2095–2103. https://doi.org/10.1093/nar/24.11.2095.

47. Sinha, R., and Khare, S.K. (2014). Protective role of salt in catalysis and maintaining structure of halophilic proteins against denaturation. Front. Microbiol. *5*, 165. https://doi.org/10.3389/fmicb.2014.00165.

48. Düster, R., Kaltheuner, I.H., Schmitz, M., and Geyer, M. (2021). 1,6-Hexanediol, commonly used to dissolve liquid–liquid phase separated condensates, directly impairs kinase and phosphatase activities. J. Biol. Chem. *296*, 100260. https://doi.org/10.1016/j.jbc.2021.100260.

49. Otzen, D.E., Pedersen, J.N., Rasmussen, H.Ø., and Pedersen, J.S. (2022). How do surfactants unfold and refold proteins? Adv. Colloid Interface Sci. *308*, 102754. https://doi.org/10.1016/j.cis.2022.102754.

50. Hearst, J.E. (1981). Psoralen Photochemistry and Nucleic Acid Structure. J. Invest. Dermatol. *77*, 39–44. https://doi.org/10.1111/1523-1747.ep12479229.

51. Thompson, J.F., and Hearst, J.E. (1983). Structure of E. coli 16S RNA elucidated by psoralen crosslinking. Cell *32*, 1355–1365. https://doi.org/10.1016/0092-8674(83)90316-1.

52. Tauber, D., Tauber, G., Khong, A., Van Treeck, B.V., Pelletier, J., and Parker, R. (2020). Modulation of RNA Condensation by the DEAD-Box Protein eIF4A. Cell *180*, 411–426.e16. https://doi.org/10.1016/j.cell.2019.12.031.

53. Freibaum, B.D., Messing, J., Nakamura, H., Yurtsever, U., Wu, J., Kim, H.J., Hixon, J., Lemieux, R.M., Duffner, J., Huynh, W., et al. (2024). Identification of small molecule inhibitors of G3BP-driven stress granule formation. J. Cell Biol. *223*, e202308083. https://doi.org/10.1083/jcb.202308083.

54. Jain, S., Wheeler, J.R., Walters, R.W., Agrawal, A., Barsic, A., and Parker, R. (2016). ATPase-Modulated Stress Granules Contain a Diverse Proteome and Substructure. Cell *164*, 487–498. https://doi.org/10.1016/j.cell.2015.12.038.

55. Wang, T., Tian, X., Kim, H.B., Jang, Y., Huang, Z., Na, C.H., and Wang, J. (2022). Intracellular energy controls dynamics of stress-induced ribonucleoprotein granules. Nat. Commun. *13*, 5584. https://doi.org/10.1038/s41467-022-33079-1.

56. Tourrière, H., Chebli, K., Zekri, L., Courselaud, B., Blanchard, J.M., Bertrand, E., and Tazi, J. (2023). The RasGAP-associated endoribonuclease G3BP mediates stress granule assembly. J. Cell Biol. *222*, e200212128072023new. https://doi.org/10.1083/jcb.200212128072023new.

57. Rizzo, M.A., Davidson, M.W., and Piston, D.W. (2009). Fluorescent Protein Tracking and Detection: Fluorescent Protein Structure and Color Variants. Cold Spring Harb. Protoc. *2009*, pdb.top63. https://doi.org/10.1101/pdb.top63.

58. Burke, J.M., Lester, E.T., Tauber, D., and Parker, R. (2020). RNase L promotes the formation of unique ribonucleoprotein granules distinct from stress granules. J. Biol. Chem. *295*, 1426–1438. https://doi.org/10.1074/jbc.RA119.011638.

59. Yao, R.-W., Xu, G., Wang, Y., Shan, L., Luan, P.-F., Wang, Y., Wu, M., Yang, L.-Z., Xing, Y.-H., Yang, L., et al. (2019). Nascent Pre-rRNA Sorting via Phase Separation Drives the Assembly of Dense Fibrillar Components in the Human Nucleolus. Mol. Cell *76*, 767–783.e11. https://doi.org/10.1016/j.molcel.2019.08.014.

60. Decker, C.J., Burke, J.M., Mulvaney, P.K., and Parker, R. (2022). RNA is required for the integrity of multiple nuclear and cytoplasmic membraneless RNP granules. EMBO J. *41*, e110137. https://doi.org/10.15252/embj.2021110137.

61. Wang, W., Budhu, A., Forgues, M., and Wang, X.W. (2005). Temporal and spatial control of nucleophosmin by the Ran–Crm1 complex in centrosome duplication. Nat. Cell Biol. *7*, 823–830. https://doi.org/10.1038/ncb1282.

62. Pontvianne, F., Carpentier, M.-C., Durut, N., Pavlištová, V., Jaške, K., Schořová, Š., Parrinello, H., Rohmer, M., Pikaard, C.S., Fojtová, M., et al. (2016). Identification of Nucleolus-Associated Chromatin Domains Reveals a Role for the Nucleolus in 3D Organization of the A. thaliana Genome. Cell Rep. *16*, 1574–1587. https://doi.org/10.1016/j.celrep.2016.07.016.

63. Zhou, Y., Panhale, A., Shvedunova, M., Balan, M., Gomez-Auli, A., Holz, H., Seyfferth, J., Helmstädter, M., Kayser, S., Zhao, Y., et al. (2024). RNA damage compartmentalization by DHX9 stress granules. Cell *187*, 1701–1718.e28. https://doi.org/10.1016/j.cell.2024.02.028.

64. Jayabalan, A.K., Griffin, D.E., and Leung, A.K.L. (2023). Pro-Viral and Anti-Viral Roles of the RNA-Binding Protein G3BP1. Viruses *15*, 449. https://doi.org/10.3390/v15020449.

65. Cabral, S.E., Otis, J.P., and Mowry, K.L. (2022). Multivalent interactions with RNA drive recruitment and dynamics in biomolecular condensates in Xenopus oocytes. iScience *25*, 104811. https://doi.org/10.1016/j.isci.2022.104811.

66. Ripin, N., and Parker, R. (2022). Are stress granules the RNA analogs of misfolded protein aggregates? RNA *28*, 67–75. https://doi.org/10.1261/rna.079000.121.

67. Kilburn, D., Behrouzi, R., Lee, H.-T., Sarkar, K., Briber, R.M., and Woodson, S.A. (2016). Entropic stabilization of folded RNA in crowded solutions measured by SAXS. Nucleic Acids Res. *44*, 9452–9461. https://doi.org/10.1093/nar/gkw597.

68. Meyer, M.O., Yamagami, R., Choi, S., Keating, C.D., and Bevilacqua, P.C. (2023). RNA folding studies inside peptide-rich droplets reveal roles of modified nucleosides at the origin of life. Sci. Adv. *9*, eadh5152. https://doi.org/10.1126/sciadv.adh5152.

69. Mahendran, T.S., Wadsworth, G.M., Singh, A., and Banerjee, P.R. (2024). Biomolecular Condensates Can Enhance Pathological RNA Clustering. Preprint at bioRxiv. https://doi.org/10.1101/2024.06.11.598371.

70. Figley, M.D., Bieri, G., Kolaitis, R.-M., Taylor, J.P., and Gitler, A.D. (2014). Profilin 1 Associates with Stress Granules and ALS-Linked Mutations Alter Stress Granule Dynamics. J. Neurosci. *34*, 8083–8097. https://doi.org/10.1523/JNEUROSCI.0543-14.2014.

71. Smith, J., Calidas, D., Schmidt, H., Lu, T., Rasoloson, D., and Seydoux, G. (2016). Spatial patterning of P granules by RNA-induced phase separation of the intrinsically-disordered protein MEG-3. eLife *5*, 1–18. https://doi.org/10.7554/eLife.21337.

72. Mansour, F.H., and Pestov, D.G. (2013). Separation of long RNA by agarose–formaldehyde gel electrophoresis. Anal. Biochem. *441*, 18–20. https://doi.org/10.1016/j.ab.2013.06.008.

73. Tsanov, N., Samacoits, A., Chouaib, R., Traboulsi, A.M., Gostan, T., Weber, C., Zimmer, C., Zibara, K., Walter, T., Peter, M., et al. (2016). SmiFISH and FISH-quant - A flexible single RNA detection approach with super-resolution capability. Nucleic Acids Res. *44*, e165. https://doi.org/10.1093/nar/gkw784.

74. Schindelin, J., Arganda-Carreras, I., Frise, E., Kaynig, V., Longair, M., Pietzsch, T., Preibisch, S., Rueden, C., Saalfeld, S., Schmid, B., et al. (2012). Fiji: An open-source platform for biological-image analysis. Nat. Methods *9*, 676–682. https://doi.org/10.1038/nmeth.2019.

75. Mueller, F., Senecal, A., Tantale, K., Marie-Nelly, H., Ly, N., Collin, O., Basyuk, E., Bertrand, E., Darzacq, X., and Zimmer, C. (2013). FISH-quant: automatic counting of transcripts in 3D FISH images. Nat. Methods *10*, 277–278. https://doi.org/10.1038/nmeth.2406.

CellPress
OPEN ACCESS

STAR★METHODS

KEY RESOURCES TABLE

REAGENT or RESOURCE	SOURCE	IDENTIFIER
Bacterial and virus strains		
BL21(DE3)	Thermo Scientific	EC0114
Rosetta (DE3) pLysS	Millipore Sigma	70956-3
Chemicals, peptides, and recombinant proteins		
Sodium (meta)arsenite	Sigma-Aldrich	S7400-100G
Chloramphenicol	Sigma-Aldrich	C0378-25G
Ampicillin	Sigma-Aldrich	A9518-25G
Isopropyl-β-D-thiogalactopyranoside (IPTG)	Fisher Scientific	BP1755100
HEPES	Fisher Scientific	BP310-500
cOmplete™ Protease Inhibitor Cocktail, EDTA-Free, Mini, Tablets	Sigma-Aldrich	11836170001
L-Glutathione reduced	Sigma-Aldrich	G4251-10G
Ni-NTA Agarose	Fisher Scientific	R90115
Imidazole	Fisher Scientific	O3196-500
Triton X-100	Fisher Scientific	AC327371000
Urea	Sigma-Aldrich	U1250-1KG
DyLight™ 550 NHS Ester	Thermo Scientific	62263
AfeI	New England Biolabs	R0652L
BamHI-HF	New England Biolabs	R3136T
Cyanine 5-UTP (enhanced)	Enzo Life Sciences	ENZ-42506
Cyanine 3-UTP (enhanced)	Enzo Life Sciences	ENZ-42505
Fluorescein 12 UTP	Enzo Life Sciences	ENZ-42834
TURBO DNase	Invitrogen	AM2239
Polyadenylic acid	Roche	10108626001
Polycytidylic acid	Sigma-Aldrich	P4903
Polyuridylic acid	Sigma-Aldrich	P9528
Polyguanylic acid	Sigma-Aldrich	P4404
TRIzol	Thermo Scientific	15596018
Polyethylene Glycol 3350	Fisher Scientific	18-605-319
PCR grade Proteinase K	Thermo Scientific	EO0491
Proteinase K, Molecular Biology Grade	New England Biolabs	P8107S
RNase A	Thermo Scientific	EN0531
NuPAGE™ MES SDS Running Buffer (20X)	Invitrogen	NP0002
SimplyBlue™ SafeStain	Invitrogen	LC6065
Ethylenediaminetetraacetic acid	Sigma-Aldrich	E5134
Formamide	Sigma-Aldrich	4650
1 6-Hexanediol	Sigma-Aldrich	240117
4'-Aminomethyltrioxsalen hydrochloride	Sigma-Aldrich	A4330
Tricine	Sigma-Aldrich	T0377
Triethanolamine	Sigma-Aldrich	90279
ssRNA ladder	New England Biolabs	N0362S
Lipofectamine 3000	Thermo Scientific	L3000008
Carbonyl cyanide 3-chlorophenylhydrazone	Sigma-Aldrich	C2759
2-Deoxy-D-glucose	Santa Cruz Biotechnology	sc-202010A
G3Ia	Gift from Taylor Lab	Freibaum et al.[53]

(*Continued on next page*)

Continued

REAGENT or RESOURCE	SOURCE	IDENTIFIER
G3Ia'	Gift from Taylor Lab	Freibaum et al.[53]
Tween 20	Sigma-Aldrich	P9416
RNase I	Thermo Scientific	AM2294
Dextran sulfate	Fisher Scientific	S4030
E. coli tRNA	Sigma-Aldrich	R1753
Vanadyl Ribonucleoside Complex	Sigma-Aldrich	R3380
VECTAshield	Vector Laboratories	H-1000
Critical commercial assays		
Megascript	Thermo Scientific	AM1334
Megascript cleanup	Thermo Scientific	AM1908
Label IT® Nucleic Acid Labeling Kit	Mirus Bio	MIR 3200; MIR 3600; MIR 3725
Whole Plasmid Sequencing	Plasmidsaurus	N/A
Experimental models: Cell lines		
U-2 OS wt	ATCC	HTB-96
U-2-OS G3BP1-GFP	Taylor lab	Figley et al.[70]
U-2 OS mRuby-2-PABPC1	Parker lab	Burke et al.[58]
Oligonucleotides		
See Table S1 for list of smFISH and smiFISH probe oligos		
Recombinant DNA		
GST-G3BP1	Yang et al.[20]	N/A
GST-EGFP-G3BP1	Yang et al.[20]	N/A
6xHis-MEG-3	Smith et al.[71]	pDC20
T7 luciferase	Promega	L4741
T7 cycb	*Drosophila* Genomics Resource Center	1295561
T7 ccr4	*Drosophila* Genomics Resource Center	4406
T7 pgc	*Drosophila* Genomics Resource Center	8512
EGFP-NPM1	Addgene	17578[61]
EGFP-β-Actin	Addgene	56421[57]
pRK793 7xHis-TEV	Addgene	8827
Software and algorithms		
ImageJ/FIJI	NIH	https://imagej.nih.gov/ij/
MatLab	Mathworks	https://www.mathworks.com/products/matlab.html
FISHquant	N/A	https://fish-quant.github.io/
R	CRAN	https://cran.r-project.org/
R studio	Posit	https://posit.co/products/open-source/rstudio/
Softworx	GE	https://download.cytivalifesciences.com/cellanalysis/download_data/softWoRx/7.2.1/ReleaseNotes_softWoRx_721.html
Deposited data		
Analysis scripts	This paper	Zenodo: https://doi.org/10.5281/zenodo.14027059
Other		
Vivaspin 20 MWCO 30 000	Cytiva	28-9323-61
GSTrap FF	Cytiva	17-5131-02

(*Continued on next page*)

CellPress
OPEN ACCESS

Continued

REAGENT or RESOURCE	SOURCE	IDENTIFIER
HiLoad 16/600 Superdex 200 pg	Cytiva	28989335
Cytiva Whatman™ Uniflo Syringe Filters, 0.2 μm PES	Fisher Scientific	09-928-062
Nupage™ 4-12% Bis-Tris Protein Gels, 1.0 mm, 12-well	Thermo Scientific	NP0322BOX
Zeba™ Spin Desalting Columns, 7K MWCO, 0.5 mL	Fisher Scientific	89882
12 mM # 1.5 round glass cover slips	Warner Instruments	cs-12r15
24 x 30 mM # 1.5 glass cover slips	Thomas Scientific	CLS-1764-2430
Press-to-seal Silicone isolator	Grace Biolabs	GBL664504-25EA

EXPERIMENTAL MODEL AND STUDY PARTICIPANT DETAILS

Bacterial cell culture

In vitro transcription vectors were obtained from the *Drosophila* Genomics Resource Center, excluding the luciferase vector, which was obtained from Promega. The GFP-G3BP1 protein purification vector was transformed into Rosetta 2(DE3)pLysS chemically competent *E. coli*. MEG-3 plasmid was transformed into BL21(DE3) chemically competent *E. coli*. Transformations were cultured on LB agar plates containing ampicillin (and chloramphenicol for Rosetta cells) at 37 °C overnight. Individual colonies were then isolated and cultured in LB containing ampicillin overnight. 25% glycerol stocks were prepared for storage at -80 °C. The remaining cells were pelleted by centrifugation, and DNA was isolated for further use. Plasmid sequences were verified by whole-plasmid sequencing (Plasmidsaurus).

Human cell culture, transfection, and oxidative stress

U-2 OS (female osteosarcoma) cells were obtained from the ATCC (HTB-96). U-2 OS cells stably expressing GFP-G3BP1 have been previously described.[70] All cells were cultured in Dulbecco's Modified Eagle's Medium (DMEM) supplemented with 10% fetal bovine serum. Antibiotics were not used. Cells were cultured at 37 °C with 5% CO2 in a humidified incubator. Cells used for microscopy experiments were cultured on sterile 12 mm,

1.5 glass coverslips (Warner Instruments). Lipofectamine 3000 (Thermo) was used for transient transfection as described in the manufacturer's workflow. 500 uM sodium arsenite dissolved in water was added directly to cultures and incubated as above for 1 hr to induce SGs.

METHOD DETAILS

G3BP1 protein purification

Full-length GFP-G3BP1 was purified using a protocol adapted from Yang et al.[20] GFP-G3BP1 expressing plasmids were expressed and purified from Rosetta 2(DE3)pLysS under native conditions. As previously described, the GFP-G3BP1 construct contains a TEV protease cleavage sequence between the N-terminal GST tag and the fusion protein.

One liter *E. coli* cultures were grown to an OD600 of ~0.8 at 37 °C before adding 600 uM IPTG. Cultures were then shifted to 16 °C for overnight induction. Cells were then pelleted the following morning, and the broth was decanted. Cell pellets were either processed immediately or stored at -80 °C for future use. Cell pellets were resuspended in lysis buffer (250 mM NaCl, 50 mM HEPES pH 7.5, 1 mM DTT, protease inhibitor) for processing. Resuspended cells were then sonicated using a 40% power cycle of 10 sec on and 20 sec off for 2 min/liter. The lysed suspension was then pelleted at 30,000 x g at 4 °C for 30 min.

Supernatants were then filtered (0.22 um) and run through prewashed, tandem 5 mL GSTrap HP columns (GE) (10 mL total bead volume). Columns were subsequently washed with 10 column volumes of lysis buffer before eluting in 10 mM glutathione (Sigma) in lysis buffer containing EDTA-free protease inhibitor. Following elution, samples were incubated with TEV protease at room temperature overnight without shaking. The cleaved protein fractions were analyzed by SDS-PAGE and pooled. Pooled samples were brought to 400 mM NaCl by adding 5 M NaCl. Samples were then concentrated using Vivaspin 20 mL 30 kDa MWCO spin concentrators (Cytiva) and 5 min spins with intermittent mechanical disruption by gentle pipetting to disrupt aggregation during concentration.

Concentrated samples were separated into pure fractions using Superdex 200 16/200 (GE) equilibrated in SEC buffer (400 mM NaCl, 50 mM HEPES pH 7.5, 1 mM DTT). Fractions were analyzed by SDS-PAGE, pooled, concentrated as above, filtered (0.22 um) at 5 mL volume before final concentration, flash frozen in liquid nitrogen, and stored at -80 °C. Final GFP-G3BP1 preparations were stored at ~266 uM and diluted to 137 mM NaCl in 50 mM HEPES pH 7.5 prior to use.

MEG-3 protein purification

Full-length 6XHIS-MEG-3 was purified using a protocol adapted from Smith et al.[71] MEG-3 plasmids were expressed and purified from Rosetta 2(DE3). One liter *E. coli* cultures were grown to an OD600 of ~0.7 at 37 °C before adding 400 uM IPTG. Cultures were then shifted to 16 °C for overnight induction. Cells were then pelleted the following morning, and the broth was decanted. Cell pellets were either processed immediately or stored at -80 °C for future use. Cell pellets were resuspended in Buffer A (500 mM NaCl, 20 mM HEPES pH 7.5, 20 mM imidazole, 10% vol/vol glycerol, 1% Triton X-100, 6 M urea, 1 mM DTT) with protease inhibitor for processing. Resuspended cells were then sonicated using a 40% power cycle of 10 sec on and 20 sec off for 2 min/liter. The lysed suspension was then pelleted at 30,000 x g at 4 °C for 30 min. Supernatants were then filtered (0.22 um), and lysate was passed over 5 mL nickel NTA agarose beads (Invitrogen). Bound protein was washed with Buffer B (1 M NaCl, 20 mM HEPES pH 7.5, 25 mM imidazole, 10% vol/vol glycerol, 1% Triton X-100, 6 M urea, 1 mM DTT) and eluted in Buffer C (1 M NaCl, 20 mM HEPES pH 7.5, 250 mM imidazole, 10% vol/vol glycerol, 1% Triton X-100, 6 M urea, 1 mM DTT). Fractions were analyzed by SDS-PAGE using 4-12% Bis-Tris gels and concentrated to 30 uM.

Following concentration, 500 ul of protein was incubated with 50 ug DyLight 550 NHS Ester (Thermo Scientific) for 1 hr to label. Excess dye was removed by three rounds of buffer exchange on 7K MWCO Zeba spin desalting columns (Thermo Scientific). The protein was then aliquoted and snap-frozen for storage.

In vitro transcription

Preexisting DNA templates encoding full-length *luciferase, cycB, pgc*, and *CCR4* were obtained from the *Drosophila* Genomics Resource Center. All RNA sequences were preceded by the T7 promoter sequence: TAATACGACTCACTATAGGGAG. Site-specific termination was achieved through endonuclease cleavage with *AfeI* for the luciferase vector or *BamHI* for all other vectors. Transcription followed a standard MEGAscript T7 Transcription kit protocol (Thermo) with a 4 hr transcription cycle at 37°C using 1 ug of linearized template. Fluorescent labeling was achieved by replacement of 50% UTP with either cy5- or cy3- labeled UTP (Enzo). The reaction was quenched by the addition of 1 ul TURBO DNase. Fluorescent RNA products were purified using the MEGAclear Transcription Clean-up Kit (Thermo). Final RNA quality was checked by denaturing agarose gel electrophoresis and NanoDrop spectrophotometry (Thermo).

Homopolymer labeling

Mixed-length homopolymers (Sigma) were labeled in cy3 or cy5 using the Label IT Nucleic Acid Labeling Kit (Mirus Bio), following the manufacturer's instructions.

Total RNA extraction

Total cellular RNA was extracted from G3BP1/2 knockout U2OS cells[12] following the standard TRIzol extraction protocol (Thermo Fisher, 15596018). Extracted RNA was resuspended in UltraPure distilled water (Invitrogen), and quality was measured by NanoDrop spectrophotometry (Thermo).

In vitro condensate formation

GFP-G3BP1::RNA or untagged G3BP1::RNA co-condensates were formed by the addition of 10 uM GFP-G3BP1 to condensation buffer (1X PBS, 10 mM MgCl2) containing 200 ng/ul total U2OS RNA and 50 ng/ul cy5-*luciferase* RNA unless otherwise stated. Samples were prepared in PCR tubes. All condensation reactions were performed at room temperature using freshly thawed GFP-G3BP1. Mg^{2+} concentration was varied without changing the concentration of other reaction constituents for magnesium titration experiments.

GFP-G3BP1::homopolymer co-condensates were formed in condensation buffer as above, using 100 ng/ul unlabeled homopolymer and 10 ng/ul cy3 or cy5 labeled homopolymer.

MEG-3::RNA co-condensates were formed in 25 mM HEPES pH 7.5, 150 mM NaCl, 10 mM $MgCl_2$, 200 ng/ul total hRNA, 50 ng/ul Fluorescein *cycb* RNA, and 50 ng/ul cy5 *luciferase* RNA. 30 uM MEG-3 was diluted to 3 uM in 25 mM HEPES pH 7.5 and subsequently added to the condensate reaction at 1/10 vol/vol to induce condensation with a final MEG-3 concentration of 300 nM.

Polyethylene glycol (PEG)-induced RNA condensation was achieved by including 10% PEG w/v 3350 in either standard condensation buffer (1X PBS, 10 mM MgCl2) or high salt condensation buffer (1X PBS, 10 mM MgCl2, NaCl added to 750 mM) before addition to 50 ng/ul cy5-*luciferase* RNA and 50 ng/ul cy3-*CycB* RNA.

Upon formation, all condensates were allowed to stabilize at room temperature for 1 hr prior to further treatment unless otherwise stated.

Enzyme treatment of co-condensates

GFP-G3BP1::RNA or MEG-3::RNA co-condensates were treated following 1 hr hardening at room temperature unless otherwise noted. Following hardening, PCR grade Proteinase K (Thermo, EO0491), RNase A (Thermo, EN0531), and Turbo DNase (Thermo, AM2238) were added to final concentrations of 0.1 u/ul, 1.43 ug/ul, and 0.28 u/ul, respectively. Control samples were diluted with an identical volume of enzyme buffer (50% glycerol, 1 mM CaCl2, 20 mM Tris-HCl pH 7.4). Samples were then incubated at room temperature for 15 min before preparation for imaging or further manipulation.

SDS-PAGE

Enzyme-treated condensates were mixed with SDS loading buffer (Final concentration: 50 mM Tris-HCl pH 6.8, 100 mM DTT, 2% SDS, 1.5 mM Bromophenol Blue, and 10% glycerol) and heated at 95 °C for 2 min. Samples were separated in Nu-PAGE 4 to 12% Bis-Tris gels (Invitrogen) run in MES SDS Running Buffer (Invitrogen) at 120 V until the dye front reached the bottom of the gel. Gels were then stained with SimplyBlue SafeStain (Invitrogen) for 1 hr. Polyacrylamide gels were then destained overnight in water. Gels were imaged using an iBright 1500 (Invitrogen).

Condensate dissolution

RNA and protein denaturants were added to matched Proteinase K treated and untreated samples. Chemical RNA denaturants (EDTA, 2 M Urea, 4 M Urea, and formamide) were added at 50 mM, 2 M, 4 M, and 20% V/V, respectively. These treatments correspond to 25%, 25%, 50%, and 20% dilution factors, respectively. Heat treatments were performed by incubating samples at 65 °C for 10 min or 95 °C for 2 min without sample dilution. Protein denaturants (hexanediol and NaCl) were added at 1.25 M, 5%, and 2%, respectively. These treatments correspond to dilution factors of 20% for each denaturant. Proteinase K treated and untreated samples were also treated with a 25% and 50% V/V dilution in UltraPure Distilled Water (Invitrogen) to control for the dilution factor. Samples were incubated for 15 min at room temperature for all dissolution treatments before preparation for microscopy or further manipulation.

In vitro crosslinking

Crosslinking of *in vitro* condensates was performed using the psoralen derivative 4' aminomethyltrioxsalen (4' AMT). 4' AMT was added to condensation buffer or PEG buffer while maintaining the final concentrations of other buffer components. Unless stated otherwise, 4' AMT was added at 10 ng/ul. For crosslinking, 10 ul of each sample was transferred to lids of microcentrifuge tubes that had been cut off to provide uniform exposure to UV and prevent absorption of small volumes. The lids were placed upside down (inner ring facing upwards) on a bed of ice to prevent evaporation during light exposure. Samples were placed ~1.5 in. from 354 nm UV bulbs and exposed for 10 min. Unless otherwise stated, samples were then treated with 50 mM EDTA to dissolve uncrosslinked RNA granules. For Proteinase K-treated samples, G3BP1 degradation was performed prior to UV exposure.

Denaturing agarose gel electrophoresis

Denaturing agarose gel electrophoresis was performed following a protocol adapted from Mansour and Pestov.[72] In short, agarose gels were prepared by melting 1% W/V agarose powder in 30 mM tricine and 30 mM triethanolamine (tri/tri) buffer. After a brief cooling period, formaldehyde was added to a final concentration of 1% V/V before casting. Condensate or RNA granule samples were prepared for electrophoresis by mixing 1:1 V/V with electrophoresis buffer (30 mM Tricine, 30 mM Triethanolamine, 50 mM EDTA, 25% glycerol, and 0.04% bromophenol blue) and incubating at 65 °C for 10 min. Gels were run in 30 mM tricine and 30 mM triethanolamine buffer at 145 V until the dye front entered the gel. The voltage was then turned down to 110 V (11 V/cm) until imaging. NEB ssRNA ladders were run alongside samples for representative images and post-stained using 1 ug/mL ethidium bromide in tri/tri buffer. Gels were imaged using an iBright 1500 (Invitrogen), visualizing cy5 and cy3 fluorescence for samples and "nucleic acid gels" mode for the ladder.

ATP depletion with G3la treatment

Cultured U2OS cells were treated with 500 uM sodium arsenite for 1 hr total, 100 uM CCCP and 200 mM 2DG for 30 min total, and 50 uM G3la for 3 min total with inclusion or exclusion of each treatment as appropriate for each experimental condition. Cells were washed once in 1X PBS, fixed in 4% formaldehyde for 15 min, washed three times in 1X PBS, and permeabilized in 1X PBST for five minutes before smFISH as below.

Permeabilization and intracellular enzyme treatment

Cultured U2OS cells were permeabilized by incubation with 0.2% Tween 20 in 1X PBS for 10 min. Cells treated with sodium arsenite were washed three times with 1X PBS prior to the addition of PBSTween. Following permeabilization, cells were gently washed once with 1X PBS. The remaining solution was then aspirated, and 0.02 u/ul Proteinase K (Molecular Biology Grade, NEB, P8107S), 100 ug/ul RNase A and 1 u/ul RNase I, or 1 u/ul Turbo DNAse were added directly to cells grown on cover glass. RNase and DNase samples were incubated for 10 min at room temperature, while Proteinase K samples were incubated for 3 min to minimize cell detachment from the cover glass. 4% formaldehyde was added directly to samples to quench enzymatic degradation and fix cells. Cells were fixed for 15 min at room temperature before performing RNA FISH.

Single-molecule (inexpensive) RNA FISH

Formaldehyde-fixed cells were washed two times in 1X PBS, followed by a short (~5 min) room temperature incubation with RNA FISH Wash A Buffer (2X SSC + 10% formamide). Samples were then incubated with 125 nM respective FISH probes in Hybridization Buffer (50% dextran sulfate, 10 mg/ml *E. coli* tRNA, 200 mM vanadyl ribonucleoside complex, 2X SSC, and 10% formamide V/V) overnight at 37 °C. Single Molecule Inexpensive FISH probes were annealed following the protocol described in Tsanov et al.[73] before use as standard smFISH probes. Samples were then washed twice in Wash A for 30 min at 37 °C, with the second

wash containing 1 ug/ml DAPI. Samples were then washed once with Wash B (2X SSC), and slides were immediately prepared and imaged.

Microscopy

All microscopic images were acquired on a PCO Edge sCMOS camera using a DeltaVision Elite inverted microscope (GE Healthcare), with an Olympus PLAN APO 60× 1.42 NA objective using SoftWorx software (Applied Precision) using 0.2μm *z*-stacks. Representative *in vitro* condensate images are presented as cropped maximum intensity projections of raw z-stack images. Representative images of smFISH experiments were deconvolved using Deltavision (SoftWorx) deconvolution software before maximum intensity projection. Images were further processed using FIJI.[74]

Slides were prepared by placing 12 mm round cover glass coated with sample face down on a larger 24 x 30 mm rectangular cover glass. The sandwiched samples were then affixed to slides using a Grace Bio-Labs silicone isolator. For smFISH samples, VECTASHIELD was added to reduce photobleaching. For in vitro condensates, no antifade was used.

QUANTIFICATION AND STATISTICAL ANALYSIS

Quantification of *in vitro* granule intensity

Experiments analyzing *in vitro* co-condensates of GFP-G3BP1 and Proteinase K-treated RNA granules were imaged with identical imaging settings between replicates to allow for comparison of granule intensities between different conditions. Using FIJI, sum intensity projections were produced from each z-stacked image, the projections were subjected to a Gaussian Blur 2 AU, and a threshold was manually set using the RNA channel to identify granules. A mask of RNA granules was separated into individual Regions of Interest (ROI). The average intensity of each ROI was measured in both RNA and protein channels. Independently, three square ROIs were defined in regions without granules to determine the background intensity in each image. The averaged background intensity was then subtracted from each granule's intensity to measure the intensity above the background. These intensities were averaged and normalized to their respective control conditions for plotting. Plots are standard box plots with vertical bars representing minimums and maximums, the 25^{th}-75^{th} percentile range plotted as a box, and the median as a horizontal line with the box. Intensity quantification was performed using n = 10 fields of view, unless otherwise stated in the figure legend.

Pelleting of *in vitro* co-condensates

20 ul GFP-G3BP1::RNA and MEG-3::RNA co-condensate reactions were made in DNA LoBind tubes (Eppendorf) as above. Samples were then quantified by Nanodrop to determine the total RNA in each reaction. Samples were then pelleted by spinning at 20,000 X g for 20 min with or without Proteinase K treatment. The supernatant was carefully removed, and the volume of the supernatant and pellet were measured by micropipette. Samples were then quantified by Nanodrop. The total RNA in the supernatant was calculated as the supernatant volume times the concentration of RNA in the supernatant sample. To account for residual supernatant, the total RNA in the pellet was calculated as the total volume of the pellet times the concentration of RNA in the pellet minus the volume of RNA in the pellet times the concentration of RNA in the supernatant. The fraction of RNA in the pellet was then quantified as the ratio of nanograms of RNA in the pellet over nanograms of RNA in total. An RNA-only solution manipulated identically was treated as a negative control. Bar plots represent the mean of n = 3 independent pelleting experiments, with each dot being an experimental data point. Error bars represent the standard deviation.

Quantification of RNA denaturing gels

Each lane of denaturing gels was segmented in FIJI by creating a rectangular ROI from just above the well to just below the migration front to quantify the total amount of RNA fluorescence. The lanes were then split into three ROIs "well," "smear," and "singlet," with any intensity below the singlet band being considered degradation products and not quantified. The well, smear, and singlet fractions were then divided by the total intensity within the lane to determine the fraction of RNA in each category. Background subtraction was performed by subtracting the average intensity of three squares past the migration front from the total intensity values of each category. Bar plots represent the mean of n = 3 independent electrophoretic experiments, with each dot being an experimental data point. Error bars represent the standard deviation.

Analysis of cellular RNA counts, localization, and intensity

NORAD counts in untreated and Proteinase K-treated cells were measured using the Matlab implementation of FISH-quant.[75] Briefly, images were cropped to include one cell, cells were manually outlined, 3D LoG filtered using default FISH-quant parameters (size = 5, s.d. = 1), spots were pre-detected with local maximum fitting, and RNAs were detected using an image-dependent intensity threshold, using sub-region fitting of 2 pixels in the *x*- and *y*-axes and 3 pixels in the *z*-axis. RNA intensity was calculated at each identified smFISH spot to generate an average *NORAD* intensity in each cell.

To overcome the loss of GFP-G3BP1 signal in Proteinase K treated cells, putative stress granules were manually masked using cytoplasmic oligo(dT) signal in both control and Proteinase K treated cells. FISHquant Identified *NORAD* smFISH spots were imported to FIJI as a multipoint selection. The number of FISH spots overlapping the cytoplasmic oligo(dT) granule masks were then counted. The fraction of spots colocalizing with oligo(dT) was then divided by the total number of FISH spots in each cell to

determine the percentage of stress granule localized *NORAD* RNA. Oligo(dT) and GFP-G3BP1 intensity were additionally calculated to generate average intensity plots.

Plots are standard box plots with vertical bars representing minimums and maximums, the 25^{th}-75^{th} percentile range plotted as a box, and the median as a horizontal line with the box. Intensity quantification was performed using n = 20 cells, unless otherwise stated in the figure legend.

Line scans

Non-punctate smFISH signals were compared between untreated and Proteinase K-treated embryos by measuring a 10-um line scan roughly centered on the middle of the RNA signal in both RNA and protein channels. 3 um from both sides of the maximum intensity were averaged to generate a line scan plot across multiple cells and granules. Line plots show the mean intensity of n = 20 granules centered on the brightest point. Ribbon shows 95% confidence intervals.